Calhoun: The NPS Institutional Archive
DSpace Repository

Theses and Dissertations 1. Thesis and Dissertation Collection, all items

1991

Magnetic fields generated by internal ocean seawater motion

Davis, Charles A.

Monterey, California. Naval Postgraduate School

http://hdl.handle.net/10945/28337

Downloaded from NPS Archive: Calhoun

Calhoun is the Naval Postgraduate School's public access digital repository for research materials and institutional publications created by the NPS community. Calhoun is named for Professor of Mathematics Guy K. Calhoun, NPS's first appointed -- and published -- scholarly author.

Dudley Knox Library / Naval Postgraduate School
411 Dyer Road / 1 University Circle
Monterey, California USA 93943

http://www.nps.edu/library

NAVAL POSTGRADUATE SCHOOL
Monterey, California

THESIS

MAGNETIC FIELDS GENERATED BY
INTERNAL OCEAN SEAWATER MOTION

by

Charles A. Davis

December, 1991

Thesis Advisor: Dr. Donald L. Walters

Approved for public release; distribution is unlimited.

T260069

REPORT DOCUMENTATION PAGE

Form Approved
OMB No 0704-0188

1a REPORT SECURITY CLASSIFICATION: UNCLASSIFIED

1b RESTRICTIVE MARKINGS

2a SECURITY CLASSIFICATION AUTHORITY

2b DECLASSIFICATION / DOWNGRADING SCHEDULE

3 DISTRIBUTION / AVAILABILITY OF REPORT: Approved for public release; distribution is unlimited.

4 PERFORMING ORGANIZATION REPORT NUMBER(S): NPS

5 MONITORING ORGANIZATION REPORT NUMBER(S)

6a NAME OF PERFORMING ORGANIZATION

6b OFFICE SYMBOL (If applicable)

7a NAME OF MONITORING ORGANIZATION

6c ADDRESS (City, State, and ZIP Code)

7b ADDRESS (City, State, and ZIP Code)

8a NAME OF FUNDING / SPONSORING ORGANIZATION

8b OFFICE SYMBOL (If applicable)

9 PROCUREMENT INSTRUMENT IDENTIFICATION NUMBER

8c ADDRESS (City, State, and ZIP Code)

10 SOURCE OF FUNDING NUMBERS

PROGRAM ELEMENT NO	PROJECT NO	TASK NO	WORK UNIT ACCESSION NO

11 TITLE (Include Security Classification): Magnetic Fields Generated by Internal Ocean Seawater Motion

12 PERSONAL AUTHOR(S): Davis, Charles A.

13a TYPE OF REPORT: Master's Thesis

13b TIME COVERED: FROM ________ TO ______

14 DATE OF REPORT (Year, Month, Day): December, 1991

15 PAGE COUNT: 80

16 SUPPLEMENTARY NOTATION: The views expressed in this thesis are those of the author and do not reflect the official policy or position of the Department of Defense or the U. S. Government.

17 COSATI CODES

FIELD	GROUP	SUB-GROUP

18 SUBJECT TERMS (Continue on reverse if necessary and identify by block number): Induced magnetic fields; Magnetic anomaly detection; Internal Waves; Boundary layer turbulence

19 ABSTRACT (Continue on reverse if necessary and identify by block number)

This thesis models induced magnetic fields from the motion of seawater in the earth's magnetic field analytically and compares the results to arctic on-the-ice magnetic fluctuation measurements. The oceans have various types of internal motions, such as internal waves and turbulence. This motion of seawater, which is a conductor, in the earth's magnetic field induces a current density. This current density, in turn, induces its own magnetic field. This thesis models internal waves and upper layer ocean turbulence analytically. The corresponding induced magnetic fields are calculated using a static form of Maxwell's equations and parameters for the Arctic are inserted. Comparisons are made with measurements from the Arctic Internal Wave Experiment (1985). The predicted fields from internal waves have magnitudes that are measurable and of the same order of magnitude as ionospherically generated fields. The predicted fields from turbulence are several orders of magnitude smaller than ionospherically generated fields. Besides giving information about internal motions in

20 DISTRIBUTION / AVAILABILITY OF ABSTRACT: ☒ UNCLASSIFIED/UNLIMITED ☐ SAME AS RPT ☐ DTIC USERS

21 ABSTRACT SECURITY CLASSIFICATION: UNCLASSIFIED

22a NAME OF RESPONSIBLE INDIVIDUAL: D. L. Walters

22b TELEPHONE (Include Area Code): 408-646-2267

22c OFFICE SYMBOL: PH/We

DD Form 1473, JUN 86

Previous editions are obsolete

S/N 0102-LF-014-6603

Block 19 (cont.)

the ocean, the seawater induced fields are a noise source in magnetic anomaly detection.

Approved for public release; distribution is unlimited.

Magnetic Fields Generated by Internal Ocean Seawater Motion

by

Charles A. Davis
Lieutenant, United States Navy
B.S., Duke University

Submitted in partial fulfillment
of the requirements for the degree of

MASTER OF SCIENCE IN PHYSICS

from the

NAVAL POSTGRADUATE SCHOOL
December 1991

Karlheinz E. Woehler, Chairman
Department of Physics

Thesis
Q169523
c.1

ABSTRACT

This thesis models induced magnetic fields from the motion of seawater in the earth's magnetic field analytically and compares the results to arctic on-the-ice magnetic fluctuation measurements. The oceans have various types of internal motions, such as internal waves and turbulence. This motion of seawater, which is a conductor, in the earth's magnetic field induces a current density. This current density, in turn, induces its own magnetic field. This thesis models internal waves and upper layer ocean turbulence analytically. The corresponding induced magnetic fields are calculated using a static form of Maxwell's equations and parameters for the Arctic are inserted. Comparisons are made with measurements from the Arctic Internal Wave Experiment (1985). The predicted fields from internal waves have magnitudes that are measurable and of the same order of magnitude as ionospherically generated fields. The predicted fields from turbulence are several orders of magnitude smaller than ionospherically generated fields. Besides giving information about internal motions in the ocean, the seawater induced fields are a noise source in magnetic anomaly detection.

TABLE OF CONTENTS

I. INTRODUCTION 1

II. BACKGROUND 5

A. OCEAN ENVIRONMENT 5

B. INTERNAL WAVES 7

C. ARCTIC UNDER ICE SEAWATER TURBULENCE 13

III. MAGNETIC SIGNATURES 15

A. PROPAGATION OF INDUCED ELECTROMAGNETIC FIELDS . 15

B. INTERNAL WAVE SIGNATURE 17

1. Geometry 17

2. Induced Magnetic Field 20

C. UNDER ICE TURBULENCE MAGNETIC SIGNATURE 34

1. Geometry 34

2. Turbulence magnetic signature 34

D. MEASURED MAGNETIC SPECTRA 39

IV. RESULTS 42

A. EVALUATION OF INTERNAL WAVE MAGNETIC FIELD MODEL 42

B. EVALUATION OF TURBULENCE MAGNETIC FIELD MODEL . 48

V. CONCLUSIONS 53

VI. RECOMMENDATIONS 55

VII. APPENDICES 57

A. CALCULATION OF INTERNAL WAVE INDUCED MAGNETIC FIELD 57

B. CALCULATION OF TURBULENCE INDUCED MAGNETIC FIELD 60

C. INTERNAL WAVE VELOCITY POWER SPECTRAL DENSITY MEASUREMENTS 62

D. 1-D TO 2-D POWER SPECTRUM CONVERSION CALCULATION 67

LIST OF REFERENCES 68

Initial Distribution List 71

Table I: Wavelength Values 16

Table II: Internal Wave Model Numerical Values (Continuum Method) 45

Table III: Internal Wave Model Numerical Values (mode structure method) 45

Table IV: Signal Characterizations 46

Table V: Turbulence Model Numerical Values 49

Figure 1: Typical Ocean Thermocline, Halocline, and Pycnocline (Gross, 1972) 6
Figure 2: Geometry of the Earth's Magnetic Field . . . 18
Figure 3: Geometry for Calculation of Internal Wave Induced Magnetic Field 19
Figure 4: AIWEX Horizontal Velocity Spectra (solid lines); Garrett-Munk Model Spectrum (dashed lines) for comparison. (Levine, et al., 1987) 24
Figure 5: Geometry for Calculation of Turbulence Induced Magnetic Field 35
Figure 6: AIWEX Power Spectra for magnetometer (Czipott, Podney, 1985) 41
Figure 7: AIWEX Model Spectrum, CEAREX Model Spectrum, and Extrapolated Spectrum for AIWEX Magnetometer Data (Continuum Method) 43
Figure 8: AIWEX Model Spectrum, CEAREX Model Spectrum, and Extrapolated Spectrum for AIWEX Magnetometer Data (Mode Structure Method) 44
Figure 9: Turbulence Model and Extrapolated AIWEX Magnetometer Spectra 51
Figure 10: AIWEX Vertical Velocity Power Spectra (McPhee, 1989) 52

I. INTRODUCTION

Seawater is a conductor situated in the earth's magnetic field. Motion of this conductor from surface waves, internal waves, turbulence, etc. produces a motional electromotive force. The resulting current density induces its own magnetic field. Understanding the production and propagation of such magnetic signatures provides information about the underlying seawater motion. Also, these induced magnetic fields are a noise source for other magnetic measurements, such as magnetic anomaly detection.

This thesis constructed analytical models of these induced fields and compared the predicted values with experimental measurements. One model considered internal wave sources and another ocean upper boundary layer turbulence. The internal wave model had versions for the Arctic and lower latitude oceans.

The internal wave model started with the mathematical derivation of a governing equation for seawater velocity from fluid mechanics. The model assumed no rotation, zero viscosity, incompressibility, and slow variation of mean density with depth. Separation of variables provided a linear differential equation for the amplitude of the vertical component of velocity. The corresponding solution and the separation of variables equations together provided an analytical model of seawater velocity, **v**. The velocity frequency dependence was then tailored to fit observed velocity spectra for either the Arctic Ocean or lower latitude oceans.

Next, the induced magnetic field was calculated. The motion of the conducting seawater with velocity **v** in the earth's magnetic field **B** (assumed constant) induces an electromotive force and causes a current density **J**. This current density **J** induces its own magnetic field **B'**. Because the frequencies involved are on the order of 10^{-3} Hz or less, displacement currents were neglected and the inductive field **B'** calculated with the Biot-Savart Law. The total induced field **B'** at a field point was calculated assuming an internal wave of infinite y-extent with wavenumber in the x-z plane. Integration over all x and y, and over z within a depth range from D_o to D yielded B'. The wavenumber dependence was removed by two different methods. In one, B' was converted to a power spectrum, transformed from a one-dimensional to a two-dimensional spectrum, and integrated over wavenumber from a minimum, k_{min}, to infinity to give $B'^2(\omega)$. In the other, application of a boundary condition to the vertical component of velocity produced a dispersion relation between ω and k_x. Choosing the lowest mode of oscillation, using the dispersion relation, and converting to a power spectrum yielded $B'^2(\omega)$.

Data from the Arctic Internal Wave Experiment (AIWEX) in 1985 provided a means to compare the model B'^2 power spectral density as a function of frequency with experimental results. The predicted magnitudes for the induced fields B'^2 were in the same range as extrapolated magnetometer measurements. The large spatial extent of internal waves produced signals of the same order of magnitude as ionospherically generated signals. The first k-dependence method yielded frequency responses that do not follow the $1/f^2$ dependence of the data. The second method does yielded the $1/f$ or $1/f^2$ frequency dependence expected. The success of the second method implied that the modal structure of the internal wave field must always be utilized in calculating the induced magnetic fields.

The turbulence induced magnetic field model had a similar formulation. It assumed the region of turbulent seawater resides in the upper boundary layer of the ocean between depths D_o and D, and to be three dimensionally isotropic within this region. The seawater velocity **v** was analytically modeled as a linear superposition of plane waves propagating in three dimensions with various wavenumbers and frequencies. This motion in the earth's magnetic field **B** resulted in the current density **J**, which was utilized in the Biot-Savart Law to calculate the induced magnetic field **B'** at a field point, again neglecting displacement current. The total field was found by integrating over all x and y, and over z between D_o and D. Keeping the principal term of the **B'** expression, the induced field components were integrated over wavenumber from a minimum, k_{min}, to infinity. Then the horizontal field magnitude, B'_H, was converted to a power spectral density as a function of frequency.

This power spectrum was compared to the AIWEX magnetometer data. The frequency dependence of the model agreed with the observed $1/f^2$ dependence of the data. However, the predicted magnitudes were several orders of magnitude below the data. The AIWEX signal in the 10^{-1}-10^{-2} Hz range appeared to arise from fields generated in the ionosphere.

II. BACKGROUND

A. OCEAN ENVIRONMENT

The conductivity of seawater principally derives from dissolved salts. In general, conductivity decreases with depth. An average value for ocean conductivity is 4 (S/m).

Seawater density varies in the ocean. Temperature and salinity are the main governing factors. Density as a function of depth generally displays three zones (Gross, 1971). In the surface zone, from the surface to 50-100 m, the density remains approximately constant with depth due to mixing of the upper layer of ocean by wave action. The next zone, from 50-100 m to around 500-1000 m, forms the pycnocline zone. Density increases rapidly with depth. Generally, the density follows a monotonic increase because the temperature declines with depth. The bottom zone, below the pycnocline, is called the deep zone. Here, density slowly increases with depth due to decreasing temperature. Fig. 1 (Gross, 1971) depicts these zones and their general temperature, salinity, and density variations.

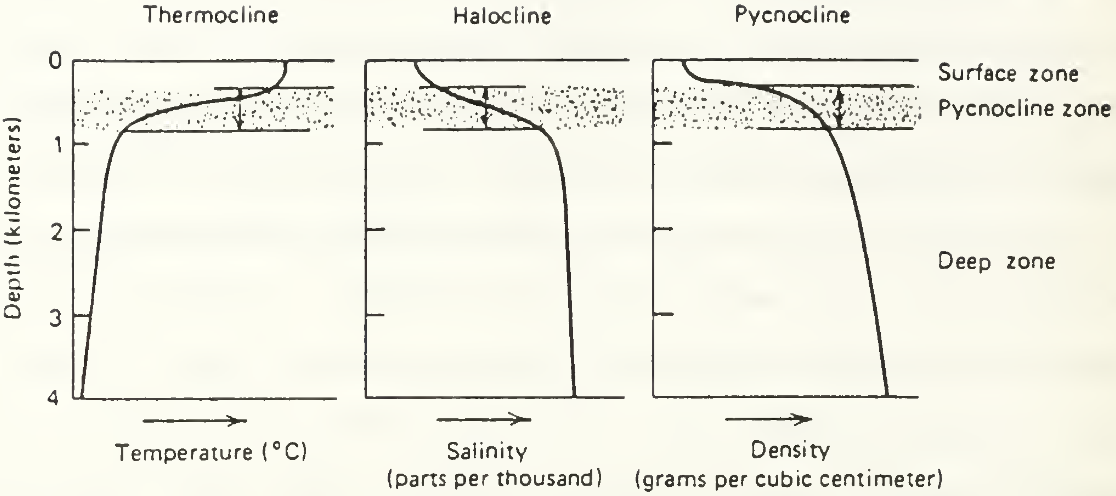

Figure 1: Typical Ocean Thermocline, Halocline, and Pycnocline (Gross, 1972)

The earth's permanent magnetic field permeates the oceans. Since the field is approximately that of a magnetic dipole, the direction and magnitude of the field vary across the oceans. It goes from basically horizontal with respect to the surface of the earth and magnitude of about 30,000 gamma (nanotesla) near the equator, to basically vertical with magnitude of about 60,000 gamma at the north and south magnetic poles. Seawater motions of the ocean within this field induce the electromotive force and the resulting current density **J**.

B. INTERNAL WAVES

A change in density with depth ($\partial\rho/\partial z < 0$) allows buoyancy oscillations within the ocean known as internal waves. The momentum and continuity equations for fluids are used to derive an equation for the vertical velocity of these internal waves.

Following Gill (1982), the fluid momentum equation is

$$\frac{D\boldsymbol{u}}{Dt}+2\Omega\times\boldsymbol{u}=-\rho^{-1}\nabla p-\boldsymbol{g}+\nu\nabla^2\boldsymbol{u}, \tag{1}$$

where $\mathbf{u}$ = fluid velocity = $u\mathbf{i} + v\mathbf{j} + w\mathbf{k}$, Ω = system rotation angular velocity, and ν = kinematic viscosity. Assume isentropic motion, i.e. no viscous effects ($\nu=0$) and no rotation ($\Omega=0$). The mass equation of continuity is

$$\rho^{-1}\frac{D\rho}{Dt} + \nabla\cdot\boldsymbol{u} = 0.$$

Assume density is a function of potential temperature, θ, and salinity, s, independent of pressure, p. Using the chain rule and taking θ and s constant with respect to time over a differential element

$$\frac{D\rho}{Dt} = \frac{\partial\rho}{\partial\theta}\frac{D\theta}{Dt} + \frac{\partial\rho}{\partial s}\frac{Ds}{Dt} = 0. \tag{3}$$

The continuity equation then becomes the incompressible fluid condition

$$\nabla \cdot \boldsymbol{u} = 0. \tag{4}$$

Assume small perturbations in pressure, p', and density, ρ',

$$p = p_o + p', \qquad \rho = \rho_o + \rho', \qquad \frac{dp_o}{dz} = -g\rho_o. \tag{5}$$

The fluid momentum equation becomes

$$\rho \frac{\partial \boldsymbol{u}}{\partial t} = -\nabla p' - \rho' g \hat{\boldsymbol{k}}. \tag{6}$$

Applying the convective derivative with average velocity **v**, the time derivative of density becomes

$$\frac{D\rho}{Dt} = \frac{\partial \rho}{\partial t} + (\boldsymbol{v}\cdot\nabla)\,\boldsymbol{v} = \frac{\partial \rho'}{\partial t} + w\frac{d\rho_o}{dz} = 0. \tag{7}$$

The fluid velocity components u and v can be eliminated by first taking the partial derivative with respect to time of the continuity equation

$$\frac{\partial}{\partial t}\nabla \cdot \boldsymbol{u} = \frac{\partial^2 u}{\partial t \partial x} + \frac{\partial^2 v}{\partial t \partial y} + \frac{\partial^2 w}{\partial t \partial z} = 0, \tag{8}$$

and then using Equation 6 in component form to replace time derivatives of u,v with spatial derivatives of p'. The result is

$$\rho_o \frac{\partial^2 w}{\partial z \partial t} = \frac{\partial^2 p'}{\partial x^2} + \frac{\partial^2 p'}{\partial y^2}. \tag{9}$$

Combining Equation [7] and the time derivative of the z-component of Equation [6] yields

$$\frac{\partial^2 w}{\partial t^2} + N^2 w = -\frac{1}{\rho_o} \frac{\partial^2 p'}{\partial z \partial t}, \tag{10}$$

where N is the Brunt-Väisälä frequency, given by

$$N^2 = -\frac{g}{\rho_o} \frac{d\rho_o}{dz}. \tag{11}$$

Taking the horizontal Laplacian of Equation [10]

$$\frac{\partial^2}{\partial t^2}\left(\frac{\partial^2}{\partial x^2} + \frac{\partial^2}{\partial y^2}\right) w + N^2 \left(\frac{\partial^2}{\partial x^2} + \frac{\partial^2}{\partial y^2}\right) w = -\frac{1}{\rho_o}\left(\frac{\partial^2}{\partial x^2} + \frac{\partial^2}{\partial y^2}\right) \frac{\partial^2 p'}{\partial z \partial t}. \tag{12}$$

Substituting Equation [9] in the right hand side and rearranging yields an equation for w, the z-component of velocity,

$$\frac{\partial^2}{\partial t^2}\left[\frac{\partial^2}{\partial x^2} + \frac{\partial^2}{\partial y^2} + \frac{1}{\rho_o} \frac{\partial}{\partial z}\left(\rho_o \frac{\partial}{\partial z}\right)\right] w + N^2 \left(\frac{\partial^2}{\partial x^2} + \frac{\partial^2}{\partial y^2}\right) w = 0. \tag{13}$$

Assume that the vertical velocity, w, varies with depth, z, much more rapidly than the density, ρ_o. Then

$$\frac{1}{\rho_o} \frac{\partial}{\partial z}\left(\rho_o \frac{\partial}{\partial z}\right) w \sim \frac{\partial^2 w}{\partial z^2}, \tag{14}$$

which is known as the Boussinesq approximation.

Equation [13] then simplifies to

$$\frac{\partial^2}{\partial t^2}\left[\frac{\partial^2}{\partial x^2}+\frac{\partial^2}{\partial y^2}+\frac{\partial^2}{\partial z^2}\right]w + N^2\left(\frac{\partial^2}{\partial x^2}+\frac{\partial^2}{\partial y^2}\right)w = 0. \qquad \textbf{(15)}$$

This equation describes the behavior of the vertical velocity component of an internal wave disturbance.

Separation of variables can simplify Equation [15]

$$w(x,y,z,t) = X(x)\ Y(y)\ Z(z)\ T(t). \qquad \textbf{(16)}$$

The X, Y, and T portions have the form

$$\frac{\partial^2 X}{\partial x^2} + k_x X = 0, \qquad \textbf{(17)}$$

with the following solutions

$$X = X_o e^{ik_x x}; \qquad Y = Y_o e^{ik_y y}; \qquad T = T_o e^{i\omega t}. \qquad \textbf{(18)}$$

The z part becomes

$$\frac{\partial^2 Z}{\partial z^2} + k_z^2\left(1-\frac{N(z)^2}{\omega^2}\right)\ Z = 0. \qquad \textbf{(19)}$$

This equation possesses the Sturm-Liouville form. Thus, its solutions are orthogonal eigenfunctions Z(z) with real eigenvalues. The vertical velocity solutions then take the form

$$w(x,y,z,t) = Z(z)\, e^{i(k_x x + k_y y - \omega t)}. \tag{20}$$

Since they are orthogonal, any internal disturbance can be expanded as a sum of these solutions.

For Z(z), try solutions of the form

$$Z(z) = \hat{w}(z)\, e^{i k_z z}. \tag{21}$$

Substituting this into Equation [19] gives for $\hat{w}(z)$

$$\frac{d^2\hat{w}}{dz^2} + 2ik_z \frac{d\hat{w}}{dz} + \left[\left(\frac{N(z)^2 - \omega^2}{\omega^2} \right) (k_x^2 + k_y^2) - k_z^2 \right] \hat{w} = 0. \tag{22}$$

The term with $N(z)^2$ makes this, in general, a nonlinear differential equation.

To simplify this equation, approximate $\rho(z)$ as a piecewise continuous function over adjacent regions such that $\partial\rho/\partial z$ is a constant in each region. Then N(z) will be a constant in each region. Equation [22] can be solved for each region, and the solutions joined with boundary conditions specifying continuity of velocity. Alternately, approximate $\rho(z)$ by a superposition of linear slope segments each with $\partial\rho/\partial z$ equal to a constant. Then N(z) is a constant for each segment and Equation [22] is again readily solved. These approximations are seldom applicable to the real ocean (Gill, 1982) for accurate velocity profiles. However, the resulting solutions do have the general shape and the oscillating character of the profiles resulting from actual ρ(z) distributions.

With N(z) equal to a constant, Equation [22] becomes a second order, constant coefficient, linear differential equation

$$\frac{d^2\hat{w}}{dz^2} + \alpha\frac{d\hat{w}}{dz} + \beta\hat{w} = 0, \tag{23}$$

$$\text{where} \quad \alpha = 2ik_z, \qquad \beta = [(\frac{N^2 - \omega^2}{\omega^2})(k_x^2 + k_y^2) - k_z^2]. \tag{24}$$

The solutions of the characteristic equation are

$$\lambda_{\pm} = \frac{-\alpha \pm\sqrt{\alpha^2 - 4\beta^2}}{2} = -ik_z \pm i\sqrt{(\frac{N^2 - \omega^2}{\omega^2})(k_x^2 + k_y^2)} \tag{25}$$

Define δ as

$$\delta = \sqrt{(\frac{N^2 - \omega^2}{\omega^2})\ (k_x^2 + k_y^2)}. \tag{26}$$

In a stratified ocean, the maximum oscillation frequency equals the buoyancy frequency N. Thus, $\omega \le N$, and δ is real. For $\omega < N$, the general solution of equation [23] is

$$\hat{w}(z) = e^{-ik_z z}[C_1\ e^{+i\delta z} + C_2\ e^{-i\delta z}]. \tag{27}$$

Initial and boundary conditions determine the constants C1 and C2.

The vertical velocity component is then

$$w(x,y,z,t) = \hat{w}(z)\ e^{i(k_x x + k_y y + k_z z - \omega t)} = \hat{w}(z)\ e^{i(\mathbf{k}\cdot\mathbf{r} - \omega t)}. \tag{28}$$

The incompressible continuity condition, Equation [6], determines the horizontal components, u and v,

$$u(x,y,z,t) = [i\frac{\partial\hat{w}}{\partial z} - k_z\ \hat{w}]\ (\frac{k_x}{k_x^2 + k_y^2})\ e^{i(\mathbf{k}\cdot\mathbf{r} - \omega t)}, \tag{29}$$

$$v(x,y,z,t) = [i\frac{\partial\hat{w}}{\partial z} - k_z\ \hat{w}]\ (\frac{k_x}{k_x^2 + k_y^2})\ e^{i(\mathbf{k}\cdot\mathbf{r} - \omega t)}. \tag{30}$$

These analytical expressions for the seawater velocity now facilitate calculating the induced magnetic fields.

C. ARCTIC UNDER ICE SEAWATER TURBULENCE

In the arctic, turbulent seawater flow exists from below the ice (effectively zero depth) down to some depth, D, at which the motion transitions to internal waves. 40 m is a typical value for D (private communication with T. Stanton).

Utilize superposition of three-dimensional plane waves of varying wavenumber and angular frequency, ω, to model this turbulent region

$$\mathbf{v} = [v_x(k_x,\omega)^{ik_x x}\hat{\boldsymbol{\imath}} + v_y(k_y,\omega)e^{ik_y y}\hat{\boldsymbol{\jmath}} + v_z(k_z,\omega)e^{ik_z z}\hat{\mathbf{k}}]\ e^{-i\omega t}. \quad \textbf{(31)}$$

Assume three-dimensional isotropy of turbulence to simplify the analysis

$$v_x(k_x,\omega) = v_y(k_y,\omega) = v_z(k_z,\omega) \equiv v(k,\omega). \quad \textbf{(32)}$$

Empirically model the velocity amplitude function $v(k,\omega)$ as

$$v(k,\omega) = \frac{v_o}{\sqrt{k_o^2 + k^2}\ \sqrt{\omega_o^2 + \omega^2}}. \quad \textbf{(33)}$$

The power spectrum for this function is then

$$v^2(k,\omega) = \frac{v_o^2}{(k_o^2 + k^2)\ (\omega_o^2 + \omega^2)}. \quad \textbf{(34)}$$

The constant factors k_o and ω_o in the denominator keep the power finite as k and ω approach zero. For large k, this exhibits the same k^{-2} dependence as for internal waves (Garret, Munk, 1972). For large ω, this exhibits the ω^{-2} dependence characteristic of under ice internal wave fields (ONR Report, 1991). The velocity expression is

$$\mathbf{v}(k,\omega,\mathbf{r},t) = \frac{v_o}{\sqrt{k_o^2 + k^2}\sqrt{\omega_o^2 + \omega^2}}\ e^{i(\mathbf{k}\cdot\mathbf{r} - \omega t)}. \quad \textbf{(35)}$$

III. MAGNETIC SIGNATURES

A. PROPAGATION OF INDUCED ELECTROMAGNETIC FIELDS

This model neglected attenuation due to the propagation of the electromagnetic waves through seawater, a conductor, because of the low frequencies involved and the corresponding long wavelengths. The electromagnetic waves are characterized by their wavelength, λ. For a "good conductor", like seawater, and a "good insulator", like air, the wavelengths are

$$\lambda_{conductor} \approx \frac{2\pi}{\sqrt{\pi\mu_o\sigma f}}, \qquad \lambda_{insulator} \approx \frac{c}{f}, \tag{36}$$

where

$$\mu_o = 4\pi x10^{-7}\frac{N}{A^2}, \qquad \sigma = cond = 4\frac{S}{m}, \qquad c = 3.0x10^{8}\frac{m}{s}. \tag{37}$$

Table I lists wavelength values for typical frequencies of interest in internal ocean seawater motions.

Table I: Wavelength Values

Freq (Hz)	$\lambda_{seawater}$ (m)	λ_{air} (m)
10^{0}	1570	3×10^{8}
10^{-1}	5030	3×10^{9}
10^{-2}	15,700	3×10^{10}
10^{-3}	50,300	3×10^{11}
10^{-4}	157,000	3×10^{12}

The induced magnetic fields will "propagate" with characteristic wavelength $\lambda_{seawater}$ up through the ocean and then with the much, much longer wavelength λ_{air} above the surface.

Characteristic ocean buoyancy frequencies are around 10^{-3} - 10^{-4} Hz. Since internal wave frequencies are always less than the buoyancy frequency, and the depth of the Arctic Ocean is around 3000 m (Dietrich, et al., 1980), the corresponding wavelengths of the induced electromagnetic radiation are much larger than the depth. Within the ocean and in the air above the ocean surface, conduction current, **J**, and not displacement current, $\epsilon \partial E/\partial t$, creates the induced magnetic field. The field point is in the "near field" and propagation effects are negligible. Relevant turbulence frequencies range around 10^{-1}-10^{-3} Hz. We confined our interest to turbulence in the upper boundary layer of the Arctic Ocean. Since a nominal depth for this layer is 40 m, the electromagnetic radiation wavelengths involved are again much larger than the depth and fields above the surface are "near field" with negligible propagation loss. Thus, we neglected attenuation due to propagation in the seawater conducting medium. For these same reasons, the sea/ice/air interfaces do not attenuate the induced fields.

The earth's magnetic field inside the ocean will possess the same value as in the air above the ocean. This follows from the assumption that the earth's field is a static (DC) field, and that the magnetic susceptibilities of the air and ocean are the same (i.e. both are non-magnetic). The equivalence derives from the resulting boundary conditions between the two media

$$B_{sea,tangential} = B_{air,tangential}, \qquad B_{sea,normal} = B_{air,normal}.$$

B. INTERNAL WAVE SIGNATURE

1. Geometry

The method of Crews and Futterman (1962) allowed us to calculate magnetic signatures. The current density followed from the seawater velocity in the earth's magnetic field. This current density was then utilized in the Biot-Savart method of calculating magnetic induction at a field point.

Fig. 2 shows the geometry of the earth's magnetic field within the ocean (northern hemisphere). To simplify the calculations, choose the wave vector in the x-z plane. Then the y-components of the wave vector and the velocity are zero. Assume the wave extends infinitely in the ±y directions. The seawater in the volume element dxdydz at the point (x,y,z) with velocity v(x,y,z,t) forms a source element for an induced magnetic field at the field point located at (0,y,-h). Fig.

3 shows this geometry. "z" represents the depth below the sea surface. "h" represents the height of the field point above the sea surface.

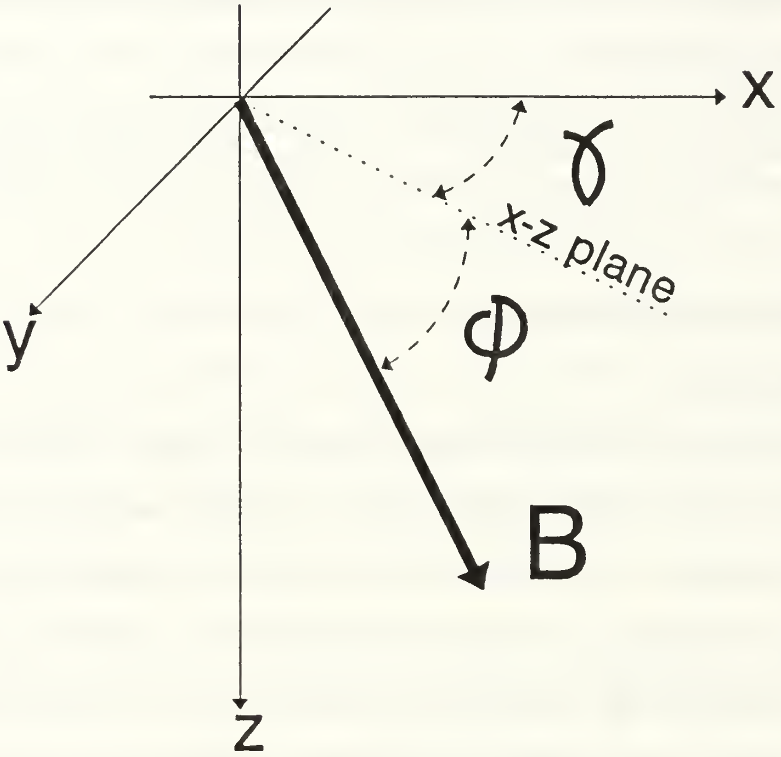

Figure 2: Geometry of the Earth's Magnetic Field

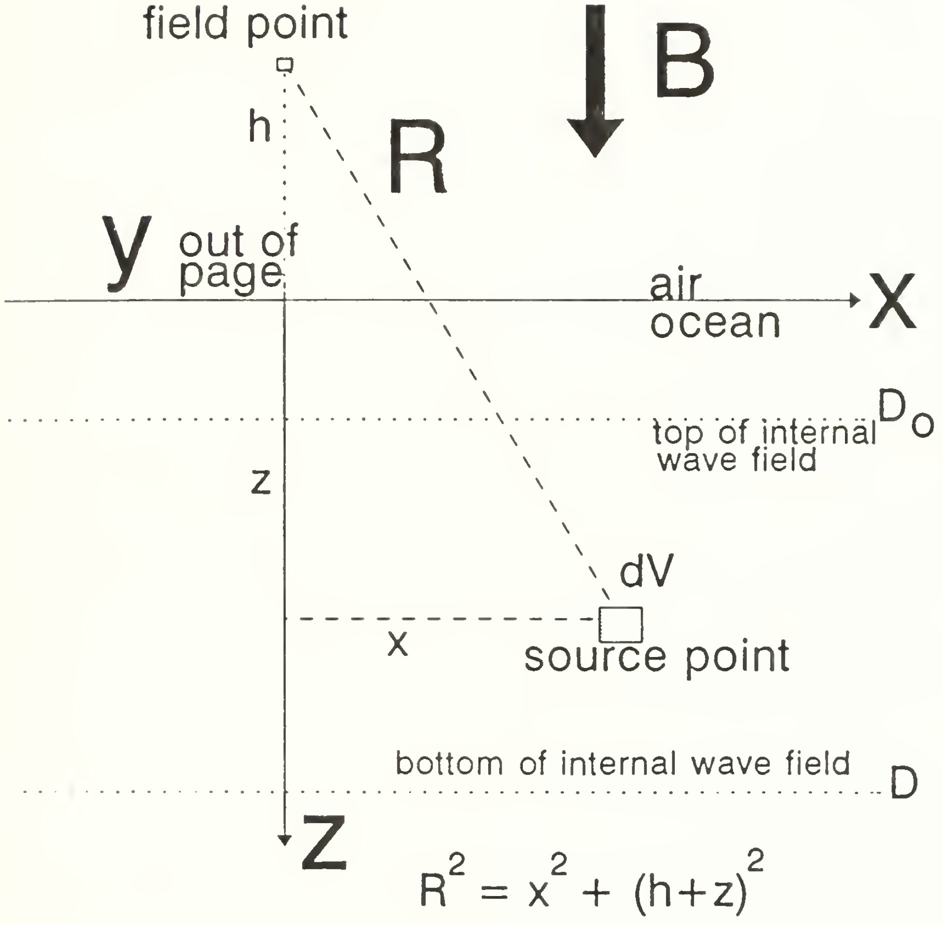

Figure 3: Geometry for Calculation of Internal Wave Induced Magnetic Field

2. Induced Magnetic Field

Seawater behaves as a relatively good conductor, with conductivity of approximately 4 S/m. The motion of this conductor in the earth's magnetic field creates an electromotive force. This in turn leads to a current density given by

$$\mathbf{J} = \sigma\ (\,\mathbf{v} \times \mathbf{B}) = \sigma\ (\,v_z B_x - v_x B_z)\ \hat{\jmath}. \qquad \textbf{(39)}$$

Since velocity is confined to the x-z plane, the current density **J** is in the y-direction.

This current density creates a secondary induced magnetic field. The Biot-Savart law gives the differential induced magnetic field due to a current element di

$$\mathbf{dB'} = \frac{\mu_o}{2\pi}\,\frac{\mathbf{di} \times \mathbf{R}}{R^2}, \qquad \mathbf{di} = \mathbf{J}\, dA. \qquad \textbf{(40)}$$

The prime indicates the secondary induced field. Integration of Equation [40] gives the components of the total induced field. The assumption of infinite extent of the wave in the ±y directions (i.e. symmetry about y=0) results in the y-component summing to zero. The x and z components are

$$B'_x = \iint dB'_x = \int_x\!\int_z \frac{\mu_o}{2\pi}\,\frac{di}{R^2}\,(h+z), \qquad \textbf{(41)}$$

$$B'_z = \iint dB'_z = \int_x\!\int_z \frac{\mu_o}{2\pi}\,\frac{di}{R^2}\,x. \qquad \textbf{(42)}$$

Substituting in the expressions for di, v, B, and R and integrating [see Appendix A] gives

$$B_x' = \frac{\mu_o B\sigma C}{2} e^{-k_x h} e^{-i\omega t} \left[\left(\frac{e^{(-k_x+i\delta)z}}{-k_x+i\delta} + \frac{e^{(-k_x-i\delta)z}}{k_x+i\delta} \right) \cos\gamma \cos\phi + \frac{\delta}{k_x} \sin\phi \left(\frac{e^{(-k_x+i\delta)z}}{-k_x+i\delta} - \frac{e^{(-k_x-i\delta)z}}{k_x+i\delta} \right) \right]_{D_o}^{D} . \tag{43}$$

$$B_z' = \frac{i\,\mu_o \sigma BC}{2} e^{-k_x h} e^{-i\omega t} \left[\left(\frac{e^{(-k_x+i\delta)z}}{-k_x+i\delta} + \frac{e^{(-k_x-i\delta)z}}{k_x+i\delta} \right) \cos\gamma \cos\phi + \frac{\delta}{k_x} \sin\phi \left(\frac{e^{(-k_x+i\delta)z}}{-k_x+i\delta} - \frac{e^{(-k_x-i\delta)z}}{k_x+i\delta} \right) \right]_{D_o}^{D} . \tag{44}$$

Here, δ reduces to

$$\delta = k_x \sqrt{\frac{N^2 - \omega^2}{\omega^2}} \quad . \tag{45}$$

These equations are fairly complicated. However, they simplify somewhat when evaluated specifically for conditions in the Arctic

$$\overline{B} = B\,\hat{k}; \qquad \phi = 90^{\circ}; \qquad \cos\phi = 0; \qquad \sin\phi = 1; \qquad D_o = 0. \tag{46}$$

The induced magnetic field components become

$$B_x' = \frac{\mu_o \sigma BC}{2} e^{-k_x h} e^{-i\omega t} (i) \sqrt{\frac{N^2-\omega^2}{\omega^2}} \left[\left(\frac{1}{-k_x+i\delta} \right) e^{(-k_x+i\delta)D} - \left(\frac{1}{k_x+i\delta} \right) e^{(-k_x-i\delta)D} - \frac{2\omega^2}{k_x (N^2-2\omega^2)} \right] . \tag{47}$$

$$B_z' = \frac{i\,\mu_o \sigma BC}{2} e^{-k_x h} e^{-i\omega t} \sqrt{\frac{N^2-\omega^2}{\omega^2}} \left[\left(\frac{1}{-k_x+i\delta} \right) e^{(-k_x+i\delta)D} - \left(\frac{1}{k_x+i\delta} \right) e^{(-k_x-i\delta)D} - \frac{2\omega^2}{k_x (N^2-2\omega^2)} \right] . \tag{48}$$

Simplifying,

$$iB_x' = B_z' = (\mu_o B\sigma C) e^{-k_x h} e^{-i\omega t} \left(\frac{1}{k_x^2+\delta^2} \right) \frac{\delta}{k_x} \left[k_x - e^{-k_x D} (-k_x \cos\delta D - \delta \sin\delta D) \right] . \tag{49}$$

Inserting the expression for δ, these become

$$iB_x'=B_z'=\mu_o B\sigma C\, e^{-k_x h}e^{-i\omega t}\frac{\omega\sqrt{N^2-\omega^2}}{k_x\, N^2}\ [1 - e^{-k_x D}(\cos\sqrt{\frac{N^2-\omega^2}{\omega^2}}\,k_x D - \sqrt{\frac{N^2-\omega^2}{\omega^2}}\sin\sqrt{\frac{N^2-\omega^2}{\omega^2}}\,k_x D)\ ]. \tag{50}$$

Note that the x and z components are exactly the same except for the phase factor of i

$$B_z' = i\, B_x', \qquad \text{with} \quad i = e^{i\frac{\pi}{2}}. \tag{51}$$

Thus, the x and z components are 90° out of phase, and the induced magnetic field vector rotates in the x-z plane. It has magnitude

$$|\boldsymbol{B}'| = |B_x'| = |B_z'| \quad . \tag{52}$$

Important characteristics of B' are (1) exponential decrease in magnitude with height, h, above the internal wave field, and (2) increase in magnitude with the vertical height D of the internal wave field.

These expressions contain angular frequency ω, wavenumber k_x, and time t. Comparison with experimental data often requires the total field power spectrum as a function of frequency. Thus, all of the wavenumber and time dependencies must be removed.

The frequency and wavenumber dependencies of the velocity were empirically modeled based on actual measurements of velocity power spectra. The amplitude of the internal wave velocity, C, which so far has only been a multiplicative component in the equations, became a function of frequency and wavenumber. This, in turn, added additional frequency and wavenumber dependence to the induced magnetic field B'.

The Arctic Internal Wave Experiment (AIWEX), conducted in 1985 in the Canada Basin of the Arctic Ocean (depth > 3500 m), measured horizontal velocity with an electromagnetic current meter at a depth of 100 m. Fig. 4 shows one such spectrum. Sampling rate limited the highest frequencies measured to around 6 cycles per hour (1.7×10^{-3} Hz), the local buoyancy frequency. The spectra indicate a 1/f frequency dependence over the range 10^{-1} - 10 cycles per hour (2.8×10^{-5} - 2.8×10^{-3} Hz) (Levine, et al.,1987). This frequency dependence was empirically modeled by

$$|\boldsymbol{v}_A|^2 = \frac{C_A^2}{\sqrt{\omega_o^2 + \omega^2}} = \frac{C_A^2}{2\pi\sqrt{f_o^2 + f^2}}, \qquad (\text{"}A\text{" for AIWEX}) \,. \tag{53}$$

For $\omega >> \omega_o$, it behaves as $1/\omega$. For $\omega < \omega_o$, its value stays approximately constant and limits the total energy in the spectrum as ω approaches zero.

The Coordinated Eastern Arctic Experiment (CEAREX) in 1989 measured velocity power spectra at depths of 50, 100,150,200, and 250 m below the surface of the ice. The 50 m measurements were made with an acoustic doppler profiler and the other measurements were made with electromagnetic current meters. Appendix C contains reproductions of the resulting velocity power spectra. All plots showed an approximately $1/f^2$ frequency dependence in the range 0.1-10 cycles per hour

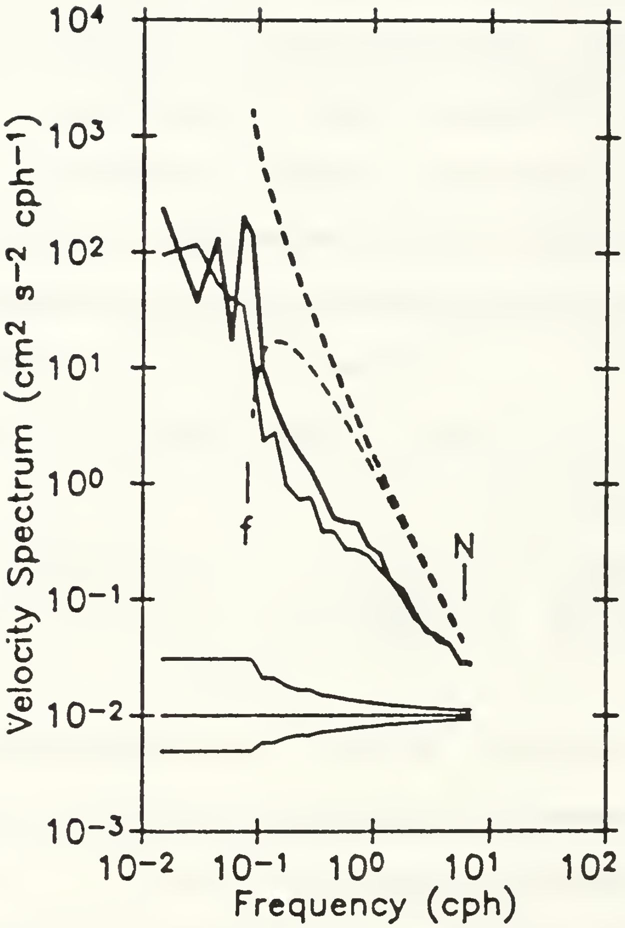

Figure 4: AIWEX Horizontal Velocity Spectra (solid lines); Garrett-Munk Model Spectrum (dashed lines) for comparison. (Levine, et al., 1987)

($2.78\text{x}10^{-5}$ - $2.78\text{x}10^{-3}$ Hz). Often this dependence flattened out for frequencies below about $4\text{x}10^{-2}$ cycles per hour ($1.11\text{x}10^{-6}$ Hz). (Czipott and Podney, 1989).

This frequency dependence was empirically modeled by

$$|v_C|^2 = \frac{C_C^2}{\omega_o^2 + \omega^2} = \frac{C_C^2}{4\pi^2(f_o^2 + f^2)}, \qquad (\text{"}C\text{" for CEAREX}). \tag{54}$$

For $\omega >> \omega_o$, it behaves as $1/\omega^2$, and for $\omega < \omega_o$, it remains approximately constant. Choosing ω_o corresponding to $4\text{x}10^{-2}$ cycles per hour gives

$$\omega_o = 2\pi f_o = 2\pi(1.11x10^{-7}\ Hz) = 7.0x10^{-7}\ rad/\text{sec}. \tag{55}$$

Measurements of internal wave spectra in other oceans of the world at lower latitudes have indicated a characteristic $1/f^2$ frequency dependence. Garrett and Munk (1971) formulated a popular empirical model based on these observations with such a frequency dependence. However, the AIWEX spectra revealed less total energy in the arctic internal wave field by factors of 15-30 than in fields described by the Garrett-Munk model (Levine, et al.,1987). The CEAREX data indicated a wavefield less energetic than lower latitude fields, but still significantly more energetic than the AIWEX wave field. The CEAREX data, due to location, were subject to large diurnal tidal motions which pumped energy into the internal wave field. In addition, under ice topography (ice keels) and local sea floor geography (i.e. Yermak plateau) affected the internal wave field (Stanton). In contrast, the AIWEX data were taken in the Canada Basin of the Arctic Ocean (Padman, et al.,1990) and experienced far more quiescent conditions.

Arctic internal wave fields possess different characteristics from lower latitude fields. Some suggested causes in the Arctic are less forcing due to wind, a damping effect caused by the ice cover, lack of surface waves, and weak large scale circulation (Levine, et al.,1987). Choice of frequency dependence in the internal wave field model critically depends on the location that is to be modeled. An arctic model will use a 1/f dependence for the velocity power spectrum, whereas a lower latitude model will use $1/f^2$. The CEAREX location represents a special situation where large tidal forcing causes the internal wave field to possess characteristics similar to lower latitude fields.

Garrett and Munk (1971) show a collection of data on displacement power spectra versus wavenumber obtained from towed measurements. The data follow a $1/k^2$ pattern over a full four decades. The largest wavenumber corresponds to a wavelength of 10,000 m. Assuming a simple plane wave description, the velocity spectrum will possess the same $1/k^2$ dependence

$$displacement = \frac{C}{\sqrt{k^2}} e^{i(kx-\omega t)}, \qquad velocity = \frac{d(displacement)}{dt} = i\omega \frac{C}{\sqrt{k^2}} e^{i(kx-\omega t)}. \tag{56}$$

A simple empirical model for the k dependence could resemble the omega dependence model with a power limiting k_o^2 factor. However, to facilitate later mathematical computations, use instead

$$|\boldsymbol{v}|^2 = \frac{C^2}{k^2}, \qquad k_{\min} < k < \infty. \quad (57)$$

The total energy in the spectrum is now limited by the cutoff at k_{min} instead of having the spectrum level out at low k. Assume this model applies to both arctic and lower latitude internal wave fields.

Combining both forms, a model for the velocity spectra for the Arctic (i.e. AIWEX) is

$$|\boldsymbol{v}_A|^2 = \frac{C_A^2}{\sqrt{\omega_o^2+\omega^2}\ k^2} = \frac{C_A^2}{2\pi\sqrt{f_o^2+f^2}\ k^2}, \qquad k_{\min}< k < \infty. \quad (58)$$

The model for lower latitude and CEAREX velocity spectra becomes

$$|\boldsymbol{v}_C|^2 = \frac{C_C^2}{(\omega_o^2 + \omega^2)\ k^2} = \frac{C_C^2}{4\pi^2(f_o^2+f^2)\ k^2}, \qquad k_{\min} < k < \infty. \quad (59)$$

Comparison with the AIWEX and CEAREX data determine the constants of proportionality, C_A and C_C. At 1 cph, the AIWEX spectrum is approximately 0.3 $(cm/s)^2/cph$ (0.11 $(m/s)^2/Hz$), and all the CEAREX spectra have approximately the value 0.5 $(cm/s)^2/cph$ (0.18 $(m/s)^2/Hz$). Approximating the AIWEX model as proportional to 1/f at this frequency

$$|\boldsymbol{v}_A|^2 = \frac{C_A^2}{2\pi f}\int_{k_{\min}}^{\infty}\frac{1}{k^2}dk = \frac{C_A^2}{2\pi f}\frac{1}{k_{\min}}, \tag{60}$$

Evaluating at 1 cph

$$|\boldsymbol{v}_A(1\ cph)|^2 = 0.3\frac{(cm/s)^2}{cph} = \frac{C_A^2}{2\pi\ (1\ cph)\ k_{\min}}, \tag{61}$$

Then

$$C_A^2 = 2\pi(0.3)\ (cm/s)^2\ k_{\min} = 1.9x10^{-4}\ k_{\min}\ (\frac{m}{s^2}). \tag{62}$$

Approximating the CEAREX model as proportional to $1/f^2$ at this frequency

$$|\boldsymbol{v}_C|^2 = \frac{C_C^2}{4\pi^2 f^2}\int_{k_{\min}}^{\infty}\frac{1}{k^2}dk = \frac{C_C^2}{4\pi^2 f^2}\frac{1}{k_{\min}}, \tag{63}$$

Evaluating at 1 cph

$$|\boldsymbol{v}_C(1\ cph)|^2 = 0.5\frac{(cm/s)^2}{cph} = \frac{C_C^2}{4\pi^2\ (1\ cph)^2\ k_{\min}}, \tag{64}$$

Then

$$C_C^2 = 4\pi^2(0.5)(cm/s)^2\text{-}cph\ \ k_{\min} = 5.5x10^{-8}\ k_{\min}\ (\frac{m}{s^3}). \tag{65}$$

The formulas for the induced magnetic field involve the velocity amplitude and not the velocity spectral density. The conversion to a velocity amplitude was made using the definition of the power spectral density. The conversion for this case was simple because of the simple time dependence.

Given a function f(t), the power spectral density is the Fourier transform of the autocorrelation function of f(t). Let F(f) be the Fourier transform of f(t). The correlation theorem says (Brigham, 1988)

$$\mathit{autocorrelation\ of}\ f(t) = \int_{-\infty}^{\infty} f(\tau)\, f(t+\tau)\, d\tau \ \leftarrow \mathit{FT\ pair} \rightarrow \ F(f)\, F^{*}(f) . \tag{66}$$

The power spectral density is thus $F(f)F^{*}(f)$. Assuming the velocity has the following time dependence

$$v(t) \equiv f(t) = C\, e^{i\omega t}, \tag{67}$$

then the Fourier transform of the velocity is

$$V(f) = \int_{-\infty}^{\infty} C\, e^{i2\pi f t} e^{i2\pi f_o t} dt = C\, \delta(f-f_o) . \tag{68}$$

The power spectral density becomes

$$|V(f)|^{2} = V(f)\, V^{*}(f) = C^{2}\, \delta^{2}(f-f_o) = C^{2} . \tag{69}$$

Thus, for this simple time dependence and real coefficient C, the power spectral density is obtained simply by squaring the coefficient.

Applying this result to the above model, the velocity becomes

$$v_A(k,\omega) = \frac{C_A}{(\omega_o^2 + \omega^2)^{1/4}\, k}, \qquad v_C(k,\omega) = \frac{C_C}{\sqrt{\omega_o^2 + \omega^2}\, k}, \qquad k_{\min} < k < \infty . \tag{70}$$

This simple model in which the frequency dependence factor and the wavenumber dependence factors are multiplicative factors makes the following calculations much easier. However, as Garrett and Munk (1971) point out, actual observations indicate that a given wavenumber's contribution depends on the frequency. Following Garrett and Munk, the function $\mu(\omega)$ was included here as a reminder of this additional frequency dependence

$$v_A(k,\omega) = \frac{C_A\,\mu(\omega)}{(\omega_o^2 + \omega^2)^{1/4}\,k}, \qquad v_C(k,\omega) = \frac{C_C\,\mu(\omega)}{\sqrt{\omega_o^2 + \omega^2}\,k}, \qquad k_{\min} < k < \infty. \quad \textbf{(71)}$$

Equation [71] replaces the constant "C" in the induced magnetic field expression, Equation [50].

Examine two different methods to remove the k-dependence. For the first method, assume internal waves exist with a continuum of frequencies from zero to the buoyancy frequency, N, and assume they possess a continuum of wavenumbers from a minimum, k_{min}, to infinity. The rationale is that actual internal wave fields result from a complex superposition of waves generated by different sources propagating in a non-uniform ocean. The assumption of a continuum may circumvent a detailed description of this wave field. The second method utilizes the eigenfunction mode structure of the wave field required by Equations [17] and [19]. Application of a boundary condition on the vertical velocity at depth D yields a dispersion relation between ω and k_x for each mode. These dispersion relations remove the k_x dependence in B'. The power spectral density B'^2 is calculated for the lowest order mode n=1. The lowest order modes will contain a majority of the energy in an internal wave field.

Try the continuum approach first. To simplify computations, assume that the depth D >> $1/k_x$. Then the last two terms in the induced magnetic field expression, which are weighted by $\exp(-k_xD)$, can be neglected with respect to 1, simplifying the conversion to power spectral densities. The induced magnetic field has the simple $e^{i\omega t}$ time dependence referred to above. Squaring the amplitude gives the corresponding power spectral density

$$|B_A'|^2 = [\mu_o B\sigma C_A]^2 \frac{1}{k_x^4} \frac{\mu^2(\omega)\ \omega^2(N^2+\omega^2)}{N^4\sqrt{\omega_o^2+\omega^2}} . \tag{72}$$

$$|B_C'|^2 = [\mu_o B\sigma C_C]^2 \frac{1}{k_x^4} \frac{\mu^2(\omega)\ \omega^2(N^2+\omega^2)}{N^4(\omega_o^2+\omega^2)} . \tag{73}$$

The formulas above are "one-dimensional" formulas in that they were derived assuming only one-dimensional wavevectors, k_x. The more general wavefield will be two-dimensional with wavevectors of magnitude

$$k = \sqrt{k_x^2+k_y^2} . \tag{74}$$

The one-dimensional expressions for the induced magnetic field power spectrum must be converted to a two-dimensional form. Yaglom (1987) shows a way to accomplish this. Given a one-dimensional power spectral density function, $f_1(k_1)$. Then the corresponding two-dimensional power spectral density function is

$$f_2(k) = -\frac{1}{\pi}\int_k^{\infty} \frac{d\,f_1(k_1)}{dk_1}\frac{dk_1}{\sqrt{k_1^2 - k^2}}. \tag{75}$$

The one dimensional induced magnetic field k dependence was $1/k_x^4$. Appendix D contains a summary of the details in computing a two dimensional k dependence. Then

$$f_2(k) = \frac{3}{4}\frac{1}{k^5}. \tag{76}$$

Now, perform the integration over k $(k_{min} < k < \infty)$

$$\int_{k_{min}}^{\infty} \frac{3}{4}\frac{1}{k^5}\,dk = -\frac{3}{16}\frac{1}{k^4}\Big|_{k_{min}}^{\infty} = \frac{3}{16}\frac{1}{k_{min}^4}. \tag{77}$$

The induced magnetic field two-dimensional power spectral density becomes

$$|B_A'|^2 = [\mu_o\sigma BC_A]^2\,\frac{3}{16\;k_{min}^4}\,\frac{\mu^2(\omega)\;(N^2-\omega^2)\,\omega^2}{N^4\sqrt{\omega_o^2+\omega^2}}, \tag{78}$$

$$|B_C'|^2 = [\mu_o\sigma BC_C]^2\,\frac{3}{16\;k_{min}^4}\,\frac{\mu^2(\omega)\;(N^2-\omega^2)\,\omega^2}{N^4(\omega_o^2+\omega^2)}. \tag{79}$$

Now apply the second method using the modal structure. Combining Equations [26],[27] and [28] gives the vertical component of velocity

$$w = (C_1e^{i\delta z} + C_2e^{-i\delta z})\;e^{i(k_xx-\omega t)}, \qquad (for\ k_y=0). \tag{80}$$

Let $C_1 = -C_2 = C/2i$. Then

$$w = C \sin(\delta z)\ e^{i(k_x x - \omega t)} . \tag{81}$$

As a boundary condition, require that the vertical velocity equal zero at the lower boundary of the internal wave field at depth D. Then

$$w\big|_{z=D} = C \sin(\delta D)\ e^{i(k_x x - \omega t)} = 0, \tag{82}$$

$$\sin(\delta D) = 0, \quad \Rightarrow \quad \delta D = \sqrt{\frac{N^2-\omega^2}{\omega^2}}\ k_x D = n\pi, \quad n=1,2.., \tag{83}$$

$$k_x = \frac{n\pi}{D}\sqrt{\frac{\omega^2}{N^2-\omega^2}}, \qquad \omega^2 = \frac{k_x^2 D^2 N^2}{n^2\pi^2 + k_x^2 D^2} . \tag{84}$$

Replace k_x in the formula for B' in Equation [50] with this dispersion relation. Taking h=0 and mode number n=1 gives

$$B' = \mu_o \sigma B C\ e^{-i\omega t}\ \frac{D}{\pi N^2}(N^2-\omega^2)\ [\ 1 + e^{-\pi\sqrt{\frac{\omega^2}{N^2-\omega^2}}}\ ] . \tag{85}$$

Converting to a power spectral density

$$B'^2 = [\mu_o \sigma B]^2 C^2 \frac{D^2}{\pi^2 N^4}(N^2-\omega^2)^2\ [\ 1 + e^{-\pi\sqrt{\frac{\omega^2}{N^2-\omega^2}}}\ ]^2 . \tag{86}$$

Model the velocity spectra with only a frequency dependence since a dispersion relation exists relating k_x to ω,

$$|v_A|^2 = \frac{C_A^2}{\sqrt{\omega_o^2 + \omega^2}}, \qquad |v_C|^2 = \frac{C_C^2}{\omega_o^2 + \omega^2}. \tag{87}$$

Replace C^2 in the B'^2 expression, Equation [86], with Equation [87]

$$|B'_A|^2 = [\mu_o \sigma B]^2 \frac{C_A^2}{\sqrt{\omega_o^2+\omega^2}} \frac{D^2}{\pi^2 N^4} (N^2-\omega^2)^2 \left[1 + e^{-\pi\sqrt{\frac{\omega^2}{N^2-\omega^2}}} \right]^2, \tag{88}$$

$$|B'_C|^2 = [\mu_o \sigma B]^2 \frac{C_C^2}{\omega_o^2+\omega^2} \frac{D^2}{\pi^2 N^4} (N^2-\omega^2)^2 \left[1 + e^{-\pi\sqrt{\frac{\omega^2}{N^2-\omega^2}}} \right]^2. \tag{89}$$

C. UNDER ICE TURBULENCE MAGNETIC SIGNATURE

1. Geometry

The same geometry as for the internal wave calculation was used, except that now the y-coordinate was important (Fig. 5). The distance R was given by

$$|\mathbf{R}| = \sqrt{x^2 + y^2 + (h+z)^2}, \quad \text{with} \quad \mathbf{R} = x\hat{\imath} + y\hat{\jmath} + z\hat{k}. \tag{90}$$

For calculational purposes, turbulence was assumed to be confined to the region $D_o<z<D$.

2. Turbulence magnetic signature

The expressions for the earth's magnetic field and the induced current density are

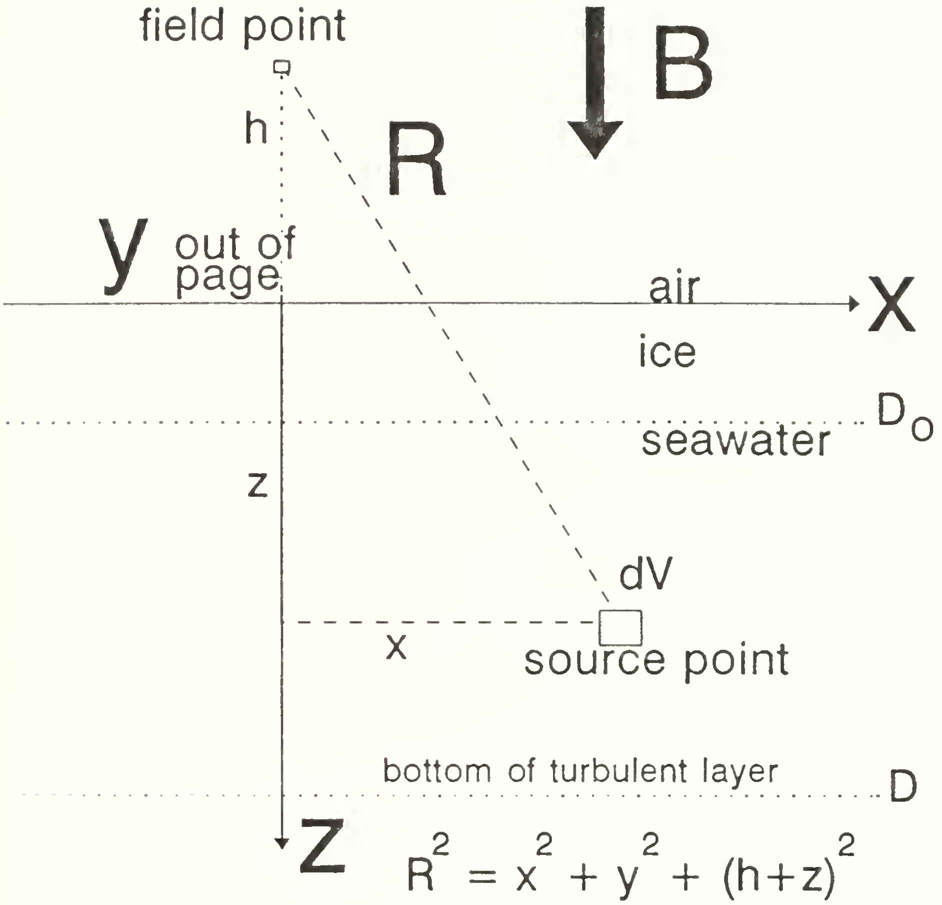

Figure 5: Geometry for Calculation of Turbulence Induced Magnetic Field

$$\boldsymbol{B} = B\,\hat{k}, \quad \text{and} \quad \boldsymbol{J} = \sigma(\boldsymbol{v} \times \boldsymbol{B})\,. \tag{91}$$

Due to the vertical direction of the magnetic field in arctic regions, the current density has only x and y components

$$\boldsymbol{J} = \sigma(v_y B\hat{i} - v_x B\hat{j})\,. \tag{92}$$

Make a change of variables for the vertical direction

$$z+h \Rightarrow z;\, dz \Rightarrow dz; \quad \text{range } D_o < z < D \Rightarrow D_o+h < z < D+h. \tag{93}$$

Then

$$\boldsymbol{J} \times \boldsymbol{R} = \sigma B[-v_x z\hat{i} - v_y z\hat{j} + (v_y y + v_x x)\hat{k}]\,. \tag{94}$$

The Biot-Savart law then gives

$$dB' = \frac{\mu_o}{4\pi}\frac{\boldsymbol{J} \times \boldsymbol{R}}{R^3}\,d^3r = \frac{\mu_o}{4\pi}\sigma B\frac{-v_x z\hat{i} - v_y z\hat{j} + (v_y y + v_x x)\hat{k}}{(x^2+y^2+z^2)^{\frac{3}{2}}}\,dxdydz. \tag{95}$$

Integration over x,y,z gives the components of the total induced magnetic field.

$$B_x' = \iiint dB_x' = \frac{\mu_o\sigma B}{4\pi}\int_{x=-\infty}^{x=\infty}\int_{y=-\infty}^{y=\infty}\int_{z=D_o+h}^{z=D+h}\frac{-v_o}{\sqrt{k_o^2+k_x^2}\sqrt{\omega_o^2+\omega^2}}\,\frac{e^{i(k_x x-\omega t)}\,z}{(x^2+y^2+z^2)^{3/2}}\,dxdydz. \tag{96}$$

The y-component equation is similar. The z-component is

$$B_z' = \iiint dB_z' = \frac{\mu_o\sigma B}{4\pi}\int_{x=-\infty}^{x=\infty}\int_{y=-\infty}^{y=\infty}\int_{z=D_o+h}^{z=D+h}\left[\frac{xe^{ik_x x}}{\sqrt{k_o^2+k_x^2}} + \frac{ye^{ik_y y}}{\sqrt{k_o^2+k_y^2}}\right]\frac{v_o\,e^{-i\omega t}}{\sqrt{\omega_o^2+\omega^2}\,(x^2+y^2+z^2)^{3/2}}\,dxdydz, \tag{97}$$

Performing the integrations [see Appendix B] yields

$$B'_x = \frac{-\mu_o \sigma B V_o e^{-i\omega t}}{2k_x\sqrt{k_o^2+k_x^2}\sqrt{\omega_o^2+\omega^2}} e^{-i\omega t} e^{-k_x h} [e^{-k_x D_o} - e^{-k_x D}], \tag{98}$$

$$B'_y = \frac{-\mu_o \sigma B V_o e^{-i\omega t}}{2k_y\sqrt{k_o^2+k_y^2}\sqrt{\omega_o^2+\omega^2}} e^{-i\omega t} e^{-k_y h} [e^{-k_y D_o} - e^{-k_y D}], \tag{99}$$

$$B'_z = \frac{i\mu_o \sigma B V_o e^{-i\omega t}}{2\sqrt{\omega_o^2+\omega^2}} [\frac{e^{-k_x h}(e^{-k_x D_o} - e^{-k_x D})}{k_x\sqrt{k_o^2+k_x^2}} + \frac{e^{-k_y h}(e^{-k_y D_o} - e^{-k_y D})}{k_y\sqrt{k_o^2+k_y^2}}]. \tag{100}$$

Approximating the geometry for an on-the-ice measurement

$$h = 0; \qquad D_o = 0; \qquad D \Rightarrow \infty. \tag{101}$$

$$B'_{x(y)} = \frac{-\mu_o \sigma B V_o e^{-i\omega t}}{2\sqrt{\omega_o^2+\omega^2}} \frac{1}{k_x\sqrt{k_o^2+k_{x(y)}^2}}, \tag{102}$$

$$B'_z = \frac{i\mu_o \sigma B V_o e^{-i\omega t}}{2\sqrt{\omega_o^2+\omega^2}} [\frac{1}{k_x\sqrt{k_o^2+k_x^2}} + \frac{1}{k_y\sqrt{k_o^2+k_y^2}}]. \tag{103}$$

Letting D approach infinity greatly simplifies the following calculations. This procedure is justified due to the expected magnitude of the parameters

$$k_x = \frac{2\pi}{\lambda} \sim \frac{2\pi}{100m}; \qquad D \sim 100-1000m; \qquad \Rightarrow e^{-k_x D} < 0.002 < 1. \tag{104}$$

These equations still have a k-dependence. To get the components as functions of only ω and t, integrate over the k-dependence

$$B_x' = \frac{-\mu_o \sigma B v_o e^{-i\omega t}}{2\sqrt{\omega_o^2+\omega^2}} \int_{k_x=k_{\min}}^{k_x=\infty} \frac{1}{k_x\sqrt{k_o^2+k_x^2}}\, dk_x, \tag{105}$$

$$= \frac{-\mu_o \sigma B v_o e^{-i\omega t}}{2\sqrt{\omega_o^2+\omega^2}} \frac{1}{k_o} \ln\left[\frac{\sqrt{k_o^2+k_{\min}^2} + k_o}{k_{\min}}\right], \tag{106}$$

where k_{min} is the smallest wavenumber (corresponding to the longest wavelength) present in the x-direction. A limit on wavelength is realistic for the ocean, and required to keep the integral finite. Recall that k_o keeps the total power finite as k approached zero. k_o thus represents the point in the power spectrum at which the characteristic k^{-2} behavior begins. k_o is thus a reasonable choice for k_{min}. Set k_{min} equal to k_o. Then

$$B_x' = \frac{-\mu_o \sigma B v_o e^{-i\omega t}}{2\sqrt{\omega_o^2+\omega^2}} \frac{\ln(\sqrt{2}+1)}{k_o}. \tag{107}$$

Similarly for the y and z components

$$B_y' = \frac{-\mu_o \sigma B v_o e^{-i\omega t}}{2\sqrt{\omega_o^2+\omega^2}} \frac{\ln(\sqrt{2}+1)}{k_o}, \quad and \quad B_z' = \frac{i\mu_o \sigma B v_o e^{-i\omega t}}{\sqrt{\omega_o^2+\omega^2}} \frac{\ln(\sqrt{2}+1)}{k_o}. \tag{108}$$

For the z-component, integration was done only over the k components which gave rise to the respective term via the Biot-Savart formula.

The total induced magnetic field is now

$$B' = |\mathbf{B}'| = \sqrt{B'^2_x + B'^2_y + B'^2_z} = \frac{\mu_o \sigma B v_o e^{-i\omega t}}{2\sqrt{\omega_o^2+\omega^2}} \frac{\ln(\sqrt{2}+1)}{k_o} \sqrt{6}\,. \qquad \textbf{(109)}$$

The horizontal component of the induced magnetic field is

$$B'_H = \sqrt{B'^2_x + B'^2_y} = \frac{\mu_o \sigma B v_o e^{-i\omega t}}{\sqrt{2}\sqrt{\omega_o^2+\omega^2}} \frac{\ln(\sqrt{2}+1)}{k_o}\,. \qquad \textbf{(110)}$$

Again, the power spectrum was obtained by Fourier transform of the autocorrelation of B', which is equivalent to squaring the amplitude here

$$B'^2 = \frac{3(\mu_o \sigma B v_o)^2 \, (\ln(\sqrt{2}+1))^2}{2\,(\omega_o^2+\omega^2)\, k_o^2}\,, \qquad \textbf{(111)}$$

$$B'^2_H = \frac{(\mu_o \sigma B v_o)^2 \, (\ln(\sqrt{2}+1))^2}{2\,(\omega_o^2+\omega^2)\, k_o^2}\,. \qquad \textbf{(112)}$$

D. MEASURED MAGNETIC SPECTRA

The Arctic Internal Wave Experiment (AIWEX) was conducted in 1985 on the arctic ice at 74°N, 145°W. In April of that year, P. Czipott and W. Podney used two induction coil magnetometers to measure the North-South horizontal component of the Earth's magnetic field. Fig. 6 shows the results from three runs. The spectra flattened out at low frequencies because the electronic gain declines at low frequencies. The region in the 10^{-2} -10^{-3} Hz decade was relatively unaffected. The spectra here showed a characteristic $1/f^2$ dependence.

They also showed an approximately hundred-fold magnitude variation between the three runs. Thus, large magnitude changes can occur over a temporal scale on the order of days. Note that the bottom spectrum basically coincides with the dashed line spectrum which corresponds to measurements made on land at Poker Flat, Alaska.

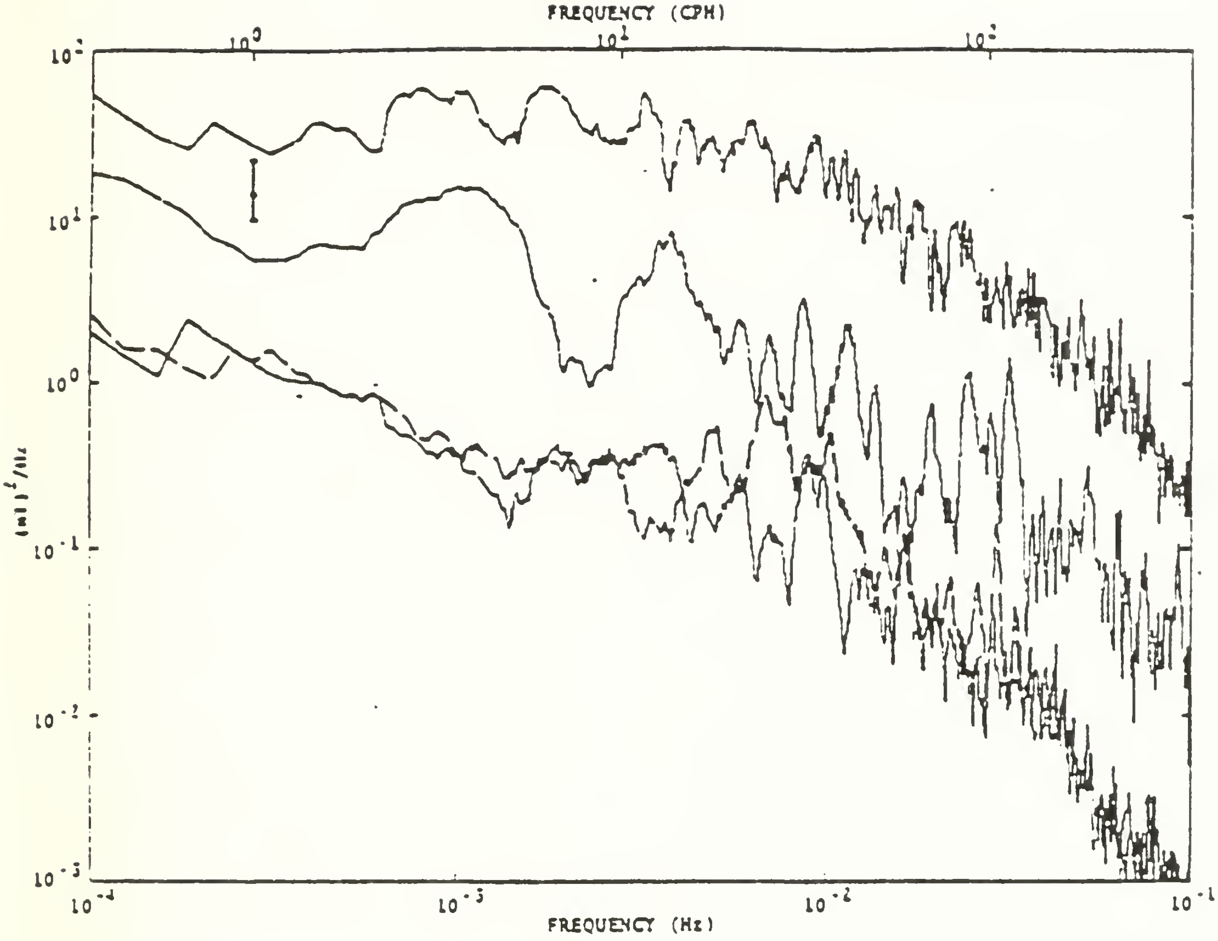

Power spectra for magnetometer output from Runs 100 (center), 103 (top), and 107 (bottom) at the ice camp, and Run 124 (dashed curve) from Poker Flat. The scale is calibrated by the magnetometer gain at 0.1 Hz: Figure 3 illustrates the dropoff in gain at lower frequency. Error bar shows the 90% confidence interval.

Figure 6: AIWEX Power Spectra for magnetometer (Czipott, Podney, 1985)

IV. RESULTS

A. EVALUATION OF INTERNAL WAVE MAGNETIC FIELD MODEL

Numerical evaluation of the formulas from the model used the following values/parameters

$$\mu_o = 4\pi x10^{-7}\ \frac{N}{A^2}; \qquad \sigma = 4.0\ \frac{S}{m}; \qquad B = 25{,}000\ nT; \tag{113}$$

$$\frac{\partial\rho}{\partial z}=3.33x10^{-3}\ \frac{kg}{m^4}; \qquad N=1.05x10^{-2}\frac{rad}{\sec}; \tag{114}$$

$$\lambda_{\max} = 10^5\ m; \qquad \Rightarrow \qquad k_{\min} = 6.28x10^{-4}m^{-1}. \tag{115}$$

Table II lists sample numerical values using the continuum ω- and k-dependence method. Table III lists sample numerical values using the modal method. For the continuum method, Fig. 7 shows the AIWEX model spectrum, the CEAREX model spectrum, and an extrapolated spectrum for the AIWEX magnetometer data. Extrapolation was made from the 10^{-1} - 10^{-2} Hz range of Run 100. Fig. 8 shows the same spectra using the modal method for the AIWEX and CEAREX models. The vertical extent, D, of the internal wave field was 300 m (D'Asaro, Morehead, 1991).

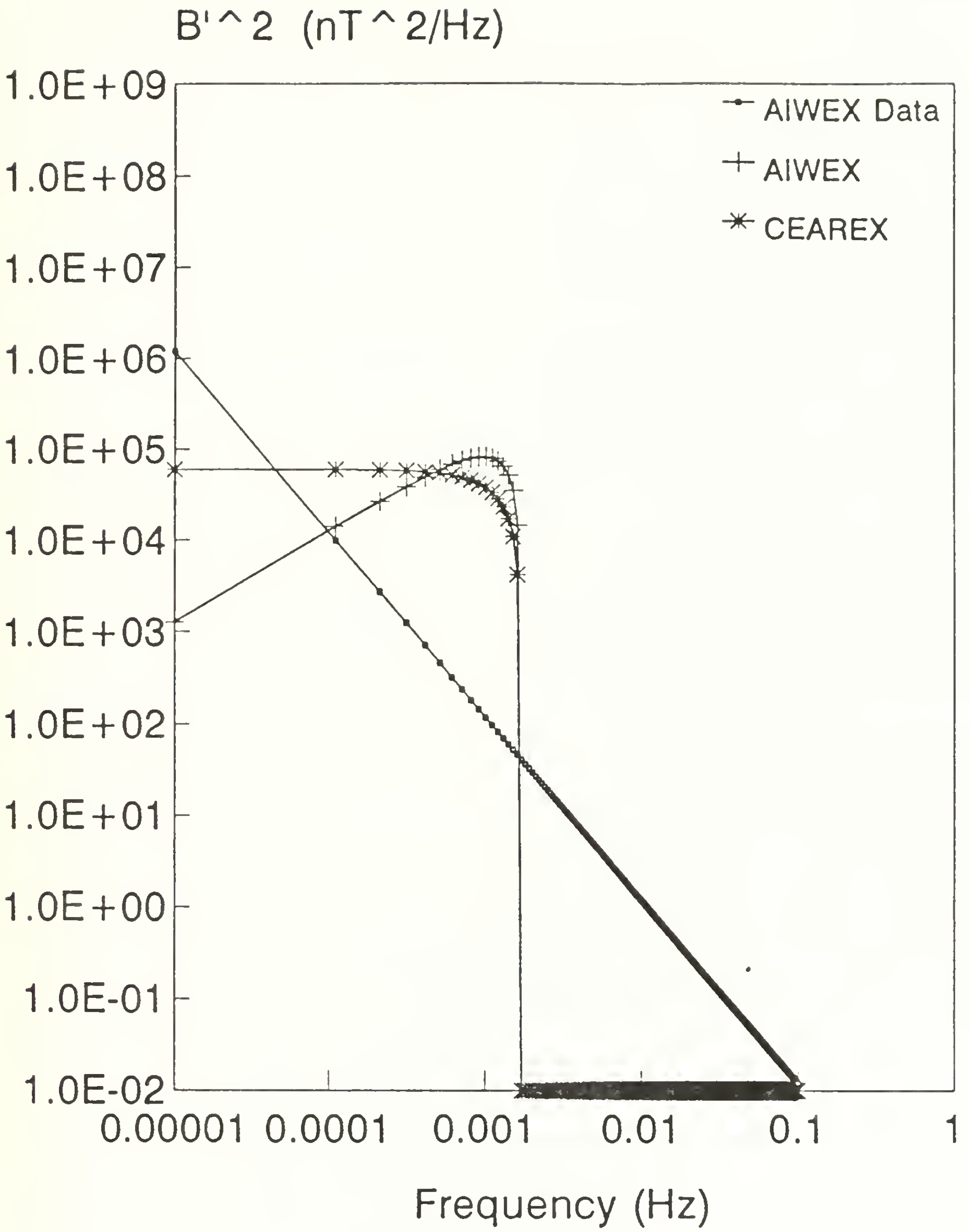

Figure 7: AIWEX Model Spectrum, CEAREX Model Spectrum, and Extrapolated Spectrum for AIWEX Magnetometer Data (Continuum Method)

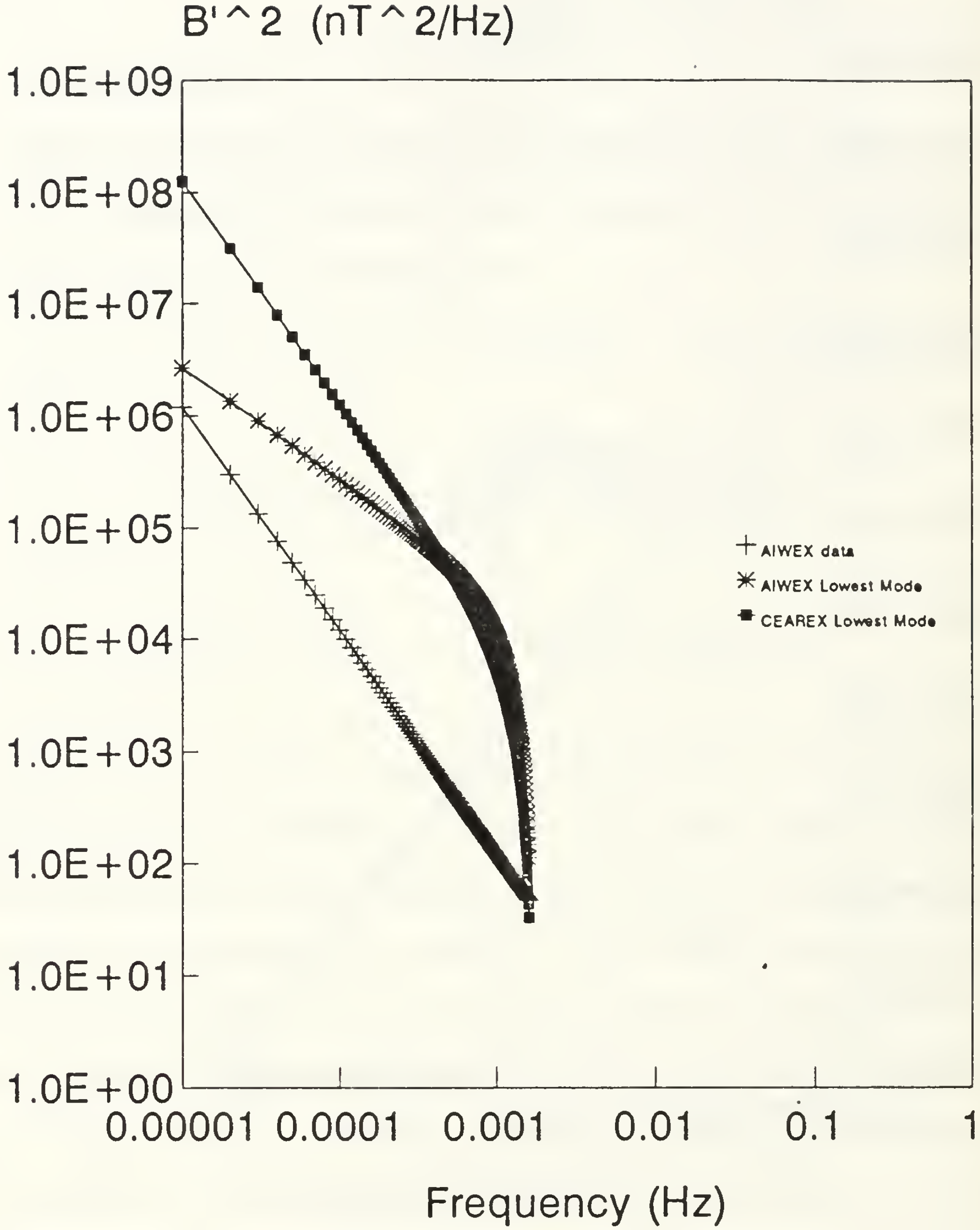

Figure 8: AIWEX Model Spectrum, CEAREX Model Spectrum, and Extrapolated Spectrum for AIWEX Magnetometer Data (Mode Structure Method)

Table II: Internal Wave Model Numerical Values (Continuum Method)

frequency (Hz)	B' AIWEX (nT^2/Hz)	B' CEAREX (nT^2/Hz)
10^{-5}	1.3×10^{3}	6.0×10^{4}
10^{-4}	1.3×10^{4}	6.0×10^{4}
10^{-3}	8.2×10^{4}	3.8×10^{4}
1.6×10^{-3}	1.7×10^{4}	4.9×10^{3}

Table III: Internal Wave Model Numerical Values (Mode Structure Method)

Frequency (Hz)	B' AIWEX (nT^2/Hz)	B' CEAREX (nT^2/Hz)
10^{-5}	2.7×10^{6}	1.3×10^{8}
10^{-4}	2.7×10^{5}	1.3×10^{6}
10^{-3}	1.1×10^{4}	5.2×10^{3}
1.6×10^{-3}	1.2×10^{2}	3.3×10^{1}

The AIWEX magnetometer measurements were not compensated for ionospherically generated magnetic fields. To separate the internal wave induced magnetic fields from the ionospheric fields, Czipott and Podney placed a tiltmeter on the ice as an independent measure of internal wave activity at the AIWEX site. They also obtained magnetograms of ionospheric activity during the experiment from several measurement stations in Alaska. Following Czipott and Podney, the signals from these three sources are compared in Table IV.

Table IV: Signal Characterizations

RUN #	IONOSPHERE (MAGNETOGRAM)	TILTMETER	MAGNETOMETER
100	"quiet"	"high"	"active"
103	"active"	"active"	"high"
105	"active"	"quiet"	"quiet"
107	"quiet"	"quiet"	"quiet"

As a first order analysis, assume the ionosphere had only two levels of activity, "quiet" and "active", measured by the magnetograms. Assume the under ice seawater motion also had only two levels of activity, "high"/"active" and "quiet", measured by the tiltmeter. Then the above four runs show the resulting magnetometer signal for the four possible combinations of ionospheric activity and seawater motion. Runs 100 and 105 indicate that the ionosphere and the seawater motion each produced a measurable magnetometer signal. Together, runs 100, 103, and 105 indicate that the magnitudes of the magnetometer and ionospheric signals were of the same order. Run 107 affirms that the magnetometer readings result from actual ionospheric and seawater motion signals.

Extrapolation of the AIWEX magnetometer data with a $1/f^2$ frequency dependence to the 10^{-3} - 10^{-5} Hz region gave power spectrum values between 10^2 and 10^6 nT^2/Hz. For the continuum method, the model values varied one to two orders of magnitude above and below these extrapolated values. The $1/k_{min}$ dependence made these continuum models sensitive to the value of k_{min} chosen. Choosing λ_{max} = 1000 m instead of 10,000 m reduced the values by an order of magnitude. For the modal method retaining only the lowest order mode, the AIWEX model predicted values one to two orders of magnitude higher than the extrapolated data, while the CEAREX model predicted values about two orders of magnitude above the extrapolated data. The mode structure model values depended on vertical extent of the internal wave field as D^2. Taking D = 100 m instead of 300 m reduced the spectra by one order of magnitude and brought them within one order of magnitude of the extrapolated data. The vertical velocity profile of Equation [81] has a simple $\sin(\delta z)$ dependence. Refining this profile could significantly reduce the energy in each mode since B'^2 is proportional to $(\text{velocity})^2$. Overall, the models reasonably predicted the magnitude of the seawater induced magnetic fields.

The frequency dependencies of the continuum models varied significantly from the $1/f^2$ dependence of the extrapolated data. The AIWEX model predicted a linear increase with frequency and then a rapid falloff as the buoyancy frequency, N, is approached. The CEAREX model predicted a parabolic falloff with frequency as $(N^2-\omega^2)$. Unfortunately, the gain falloff of the AIWEX data over internal wave frequencies may have masked any dropoff near the buoyancy frequency. These continuum models predicted too much energy at the higher frequencies. Apparently the assumption of frequency and wavenumber continua lead to erroneous predictions. The specific relation between ω and k, denoted by $\mu^2(\omega)$ in the models, must be determined. If one assumed that $\mu(\omega)$ goes as 1/(number of wavenumbers), and that number of wavenumbers was proportional to frequency (see, for example, Garrett and Munk, 1972, for a similarly modeled dependence), then the models would more closely predict the ω^{-2} dependence of the data. One could compare the internal wave model in the 10^{-1} - 10^{-2} Hz range because internal wave oscillations are limited to frequencies below the buoyancy frequency.

The mode structure method gave models with a much more realistic frequency dependence. The AIWEX model declined as 1/f before going to zero near the buoyancy frequency. This dependence paralleled the observed AIWEX velocity spectra frequency dependence. The CEAREX model fell off as $1/f^2$, just as the CEAREX velocity spectra did. These parallel frequency dependences between induced magnetic field and generating velocities satisfied physical intuition. This close correspondence between model and data implied that a proper description of internal wave induced magnetic fields requires utilizing the internal wave modal structure.

B. EVALUATION OF TURBULENCE MAGNETIC FIELD MODEL

Numerical evaluation of the formulas use the following values/parameters

$$\mu_o = 4piX10^{-7}\frac{N}{A^2}; \qquad \sigma = 4.0\ \frac{S}{m}; \qquad B = 25{,}000nT; \qquad \textbf{(116)}$$

$$v_o^2 = 5.7x10^-4\ k_o\ \frac{m^3}{Hz-s^4}; \qquad \omega_o = 2\pi x10^{-4}Hz. \qquad \textbf{(117)}$$

The v_o^2 value was determined the same way as C^2 for the internal wave model, assuming that the CEAREX data $1/f^2$ dependence extrapolates to the 10^{-1}-10^{-2} Hz range. Sample numerical values using Equation 102 are given in Table V. Fig. 9 shows a plot of the B_H' power spectral density (nT^2/Hz) versus frequency for λ_{max} = 100 m and also the extrapolated AIWEX magnetometer spectrum.

Table V: Turbulence Model Numerical Values

FREQ (Hz)	**$B'_H{}^2$(nT^2/Hz)** (λ_{max}=100 m)
10^{-3}	$4.4x10^{-6}$
10^{-2}	$4.4x10^{-8}$
$5x10^{-2}$	$1.8x10^{-9}$
10^{-1}	$4.4x10^{-10}$

The model spectra exhibited a characteristic $1/\omega^2$ dependence, just as the AIWEX data show in the 10^{-1} - 10^{-2} Hz range. However, the model values were seven orders of magnitude less than the AIWEX data. At 10^{-3} Hz the model predicted magnitude was approaching the limits of the most modern field detectors at 10^{-6} (nT^2/Hz). The smallness of the predicted signal derived from the small velocities used and the maximum characteristic wavelength of 100 m. The small velocities on the order of 10^{-1} - 10^{-3} (cm^2/s^2-Hz) were experimentally measured during AIWEX (McPhee, 1989) and their power spectrum is shown in Fig. 10. The assumption of isotropic turbulence in the model restricted wavelength values to less than about 100 m because the maximum observed depth of the upper boundary layer is about 100 m (Stanton) (note: the "average" depth is about 30-40 m). Thus, while turbulent motion in the upper boundary layer of the ocean could produce magnetic signals, the magnitude remained small because the volume of water generating the signal was limited. This implied that the AIWEX magnetometer measurements in the 10^{-1} - 10^{-3} band were due to ionospheric signal only.

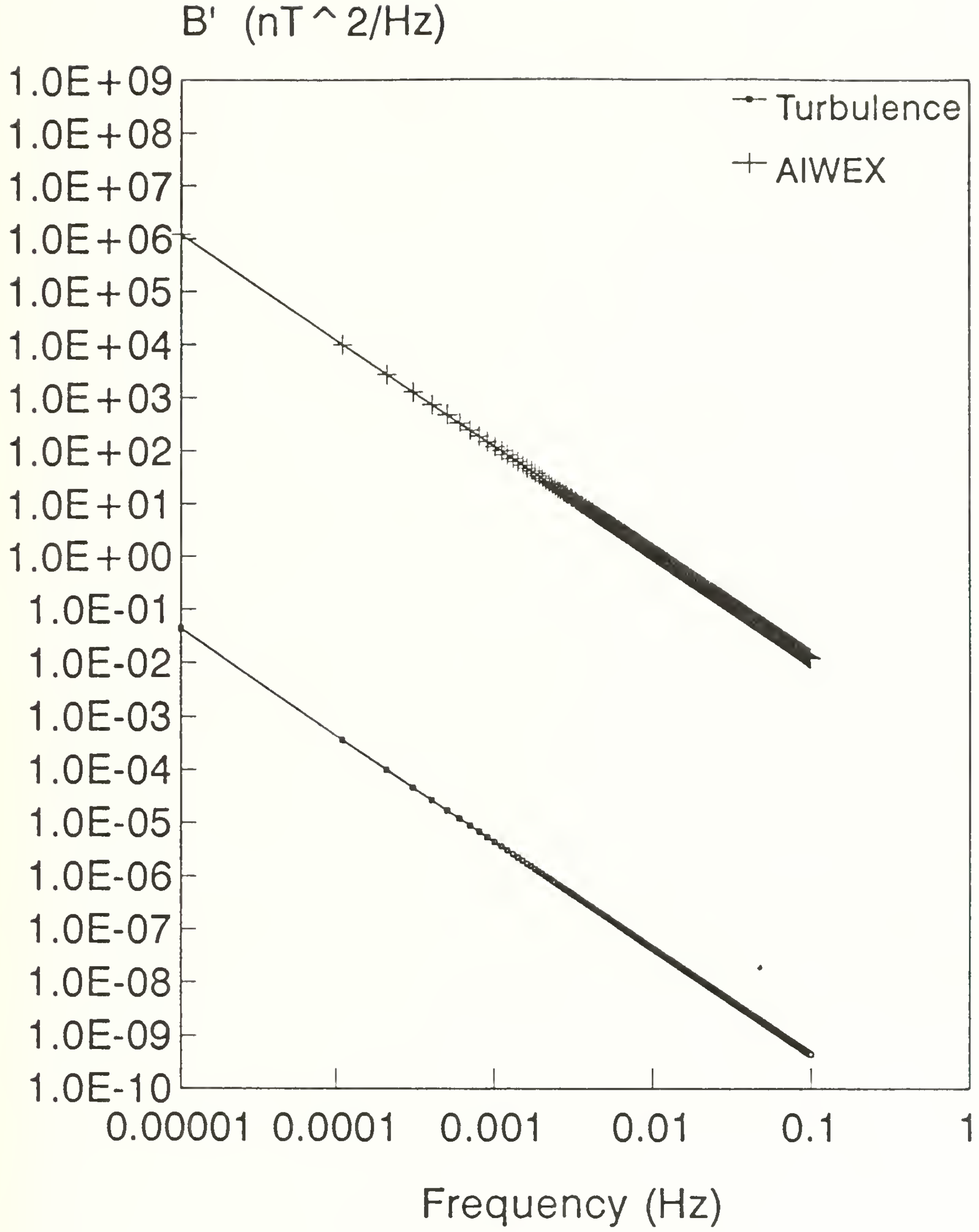

Figure 9: Turbulence Model and Extrapolated AIWEX Magnetometer Spectra

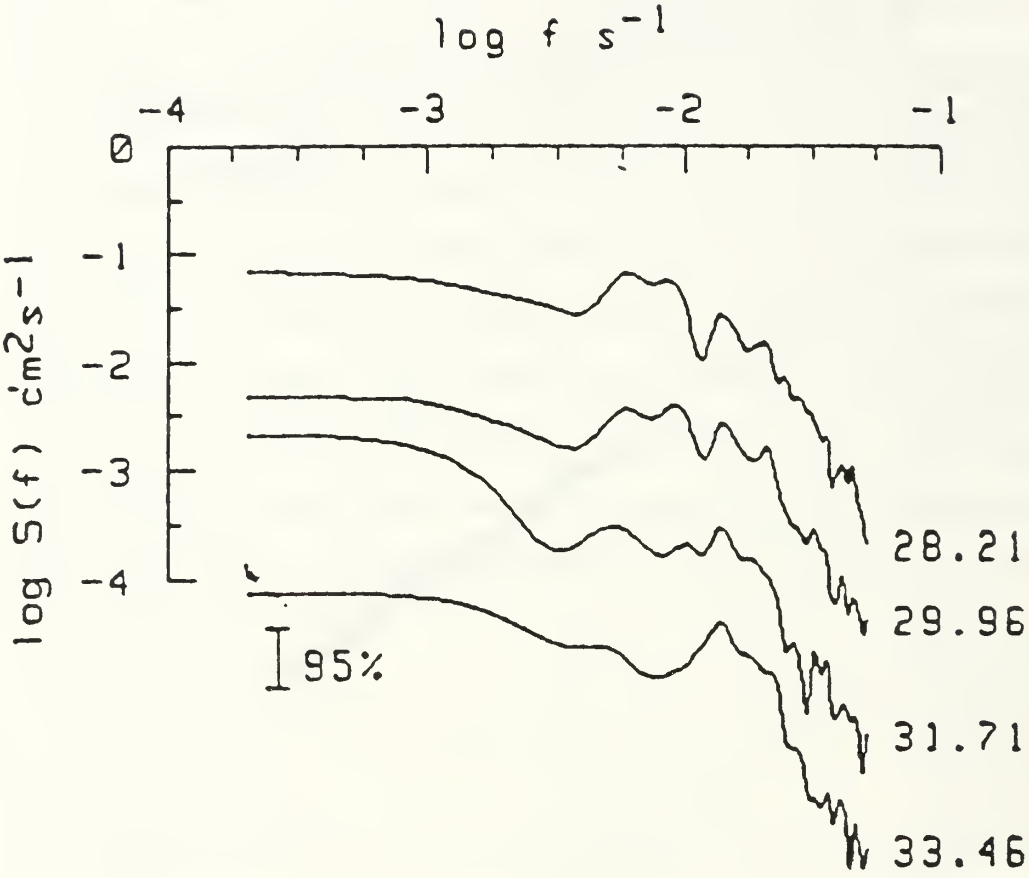

Power spectra of the vertical velocity time series at each level. The 95 percent confidence interval is shown at lower left. The spectra are plotted on log-log axes, with successive spectra displaced one decade down for clarity.

Figure 10: AIWEX Vertical Velocity Power Spectra (McPhee, 1989)

V. CONCLUSIONS

The magnetic fields induced by the motions of seawater in the earth's magnetic field were modeled analytically. Such analyses required mathematically modeling the velocities of the internal wave field and internal turbulence field, and then applying Ampere's law via the Biot-Savart formulation. For internal waves, the values predicted by the model for the induced magnetic field were roughly equal in order of magnitude to extrapolated magnetometer data. Treating internal wave frequency and wavenumber as continua yielded unphysical frequency dependences. Using an eigenmode structure for internal waves yielded more realistic frequency dependences. Thus, proper analysis of internal wave magnetic signatures must incorporate the internal wave modal structure. Additional magnetometer measurements should certify the $1/f^2$ frequency dependence and determine the behavior near the local buoyancy frequency. The turbulence model successfully coincided with magnetometer measurements in frequency dependence. The predicted frequency dependence matched the $1/f^2$ dependence of the data. However, the predicted magnitudes were several orders of magnitude below the AIWEX magnetometer measurements and approached the limits of the most sensitive magnetometers. This implied that the relatively small scale of turbulence motions (λ^{max} = 100 m) resulted in a small induced magnetic field signature. The AIWEX data in the 10^{-1} - 10^{-3} Hz range were interpreted as deriving from ionospherically generated signals .

VI. RECOMMENDATIONS

Additional measurements of seawater motion induced magnetic fields are needed. Such measurements should be made with highly sensitive magnetometers, for example, superconducting quantum interference devices (SQUIDs). Discrimination against ionospherically induced magnetic fields must be done by using the large spatial coherence length of ionospheric fields to identify and remove their signal.

The models can be extended to predict the signal seen by a gradiometer. This involves expressing the induced magnetic field at the field point in terms of field point position and taking the gradient. Gradient measurements of internal wave induced magnetic fields are more numerous than magnetometer measurements (for example, Czipott and Podney, 1985; Podney, 1975).

Both the internal wave and the turbulence models for induced magnetic field utilized the approximately vertical orientation of the earth's magnetic field in the Arctic to simplify the calculations. The models can be extended to apply the Biot-Savart calculation method to the non-vertical magnetic field at other parts of the world's oceans.

The internal wave model assumed a constant buoyancy frequency, N, for the entire wave field in the horizontal and vertical dimensions. In the actual ocean, the buoyancy frequency changes from location to location and varies significantly with depth. A more refined model must include such variations and should predict a less defined cutoff frequency due to the spread in buoyancy frequencies.

The modal version of the internal wave model should be refined by including the contributions of higher order modes. The resulting correction should not be too large because energy content rapidly declines for higher order modes due to dissipation. The velocity profiles should also be refined. As an example, require velocity continuity at the boundaries of the internal wave field and allow exponential decay outside these boundaries, analogous to going from an infinite square well solution to a finite square well solution. The amplitude within the well is reduced.

VII. APPENDICES

A. CALCULATION OF INTERNAL WAVE INDUCED MAGNETIC FIELD

For a region with constant Brunt-Väisälä frequency, N, the vertical component of the seawater velocity is given by

$$w(x,y,z,t) = \hat{w}(z)\; e^{i(\bar{k}\cdot\bar{r} - \omega t)} . \qquad (118)$$

$$\hat{w}(z) = e^{-ik_z z}\,[C_1 e^{i\delta z} + C_2 e^{-i\delta z}] . \qquad (119)$$

$$where: \qquad \delta \equiv k_x \sqrt{\frac{N^2-\omega^2}{\omega^2}} , \qquad k_y \equiv 0 . \qquad (120)$$

Require as a boundary condition

$$w(x,y,z{=}0,t) \equiv 0, \quad \Rightarrow \quad \hat{w}(z{=}0) = 1\,[C_1 + C_2], \quad \Rightarrow \quad C_1 = -C_2 \equiv C. \qquad (121)$$

Then the vertical velocity component becomes

$$\hat{w}(z) = Ce^{-ik_z z}[e^{i\delta z} - e^{-i\delta z}] . \qquad (122)$$

The derivative with respect to z is

$$\frac{\partial}{\partial z}(\hat{w}) = C(-ik_z + i\delta)\, e^{(-ik_z + i\delta)z} - C(-ik_z - i\delta)\, e^{(-ik_z - i\delta)z} . \qquad (123)$$

With the simplified geometry, the y-component of velocity is zero. The x-component of velocity becomes

$$u(x,y,z,t) = (i\frac{\partial\hat{w}}{\partial z} - k_z\hat{w})(\frac{1}{k_z})\ e^{i(\bar{k}\cdot\bar{r}\ -\ \omega t)} \tag{124}$$

$$= \frac{-C\delta}{k_x}[e^{i\delta z}+e^{-i\delta z}]\,e^{i(k_x x-\omega t)}. \tag{125}$$

These expressions can now be used to calculate the induced magnetic field

$$B_x' = \int_x\int_z \frac{\mu_o}{2\pi}\frac{di}{R^2}(h+z) \tag{126}$$

$$= \int_{x=-\infty}^{x=+\infty}\int_{z=D_o}^{z=D} \frac{\mu_o}{2\pi}\,\frac{\sigma(wB_x - uB_z)}{R^2}(h+z)\ dxdz \tag{127}$$

$$= \int_{-\infty}^{+\infty}\int_{z=D_o}^{z=D} \frac{B\mu_o\sigma C}{2\pi}\ [\frac{(e^{i\delta z}-e^{-i\delta z})\cos\gamma\cos\phi + \frac{\delta\sin\phi}{k_x}(e^{i\delta z}+e^{-i\delta z})}{(h+z)^2 + x^2}]\,e^{i(k_x x-\omega t)}[h+z]\ dzdx \tag{128}$$

The x-integration is done via contour integration in the upper half plane

$$\int_{x=-\infty}^{x=+\infty} \frac{e^{ik_x x}}{(h+z)^2 + z^2}\ dx = \oint_{UHP}\frac{e^{ik_x x}}{(x+i(h+z))(x-i(h+z))}dx - \int_{bndry}\frac{e^{ik_x x}}{(h+z)^2+z^2}dx \tag{129}$$

$$= 2\pi i[\frac{e^{ik_x(i(h+z))}}{i(h+z)+i(h+z)}] + 0 = \frac{\pi}{(h+z)}e^{-k_x(h+z)}. \tag{130}$$

Then

$$B_x' = \frac{\mu_o B\sigma C}{2} e^{-k_x h} e^{-i\omega t} \int_{D_o}^{D} (e^{(-k_x+i\delta)z} - e^{(-k_x-i\delta)z}) \cos\gamma\cos\phi + \frac{\delta\sin\phi}{k_x} (e^{(-k_x+i\delta)z} + e^{(-k_x-i\delta)z})\, dz \qquad \textbf{(131)}$$

Performing the z-integrations and noting limits of integration yields

$$B_x' = \frac{\mu_o B\sigma C}{2} e^{-k_x h} e^{-i\omega t} \; [\; [(\frac{1}{-k_x+i\delta}) e^{(-k_x+i\delta)z} + (\frac{1}{k_x+i\delta}) e^{(-k_x-i\delta)z}] \cos\gamma\cos\phi \; + \qquad \textbf{(132)}$$

$$+ \frac{\delta\sin\phi}{k_x} [(\frac{1}{-k_x+i\delta}) e^{(-k_x+i\delta)z} - (\frac{1}{k_x+i\delta}) e^{(-k_x-i\delta)z}] \;] \; \Big|_{D_o}^{D}. \qquad \textbf{(133)}$$

The z-component of the induced magnetic field is calculated similarly

$$B_z' = \int_{x=-\infty}^{x=+\infty} \int_{z=D_o}^{z=D} \frac{\mu_o}{2\pi} \frac{di}{R^2}\, x \quad = \quad \int_{-\infty}^{+\infty} \int_{D_o}^{D} \frac{\mu_o}{2\pi} \frac{\sigma(wB_x - uB_z)}{R^2}\, x\, dzdx \qquad \textbf{(134)}$$

$$= \int_{-\infty}^{+\infty} \int_{D_o}^{D} \frac{i\mu_o B\sigma C}{2\pi} [\; (e^{i\delta z} - e^{-i\delta z}) \cos\gamma\cos\phi + \frac{\delta\sin\phi}{k_x} \frac{(e^{i\delta z} + e^{-i\delta z})}{(h+z)^2 + x^2} x e^{i(k_x x - \omega t)}\, dzdx \qquad \textbf{(135)}$$

$$= \frac{i\mu_o B\sigma C}{2\pi} e^{-i\omega t} \int_{D_o}^{D} [(e^{i\delta z} - e^{-i\delta z}) \cos\gamma\cos\phi + \frac{\delta\sin\phi}{k_x} (e^{i\delta z} + e^{-i\delta z})]\, (i\pi e^{-k_x(h+z)})\, dz \qquad \textbf{(136)}$$

$$B_z' = \frac{\mu_o B\sigma C}{2} e^{-k_x h} e^{-i\omega t} \; [\; [((\frac{1}{-k_x+i\delta}) e^{(-k_x+i\delta)z} + (\frac{1}{k_x+i\delta}) e^{(-k_x-i\delta)z}) \cos\gamma\cos\phi \; + \qquad \textbf{(137)}$$

$$+ \frac{\delta\sin\phi}{k_x} [(\frac{1}{-k_x+i\delta}) e^{(-k_x+i\delta)z} - (\frac{1}{k_x+i\delta}) e^{(-k_x-i\delta)z}] \;] \; \Big|_{D_o}^{D}. \qquad \textbf{(138)}$$

Note that the x and z components have the same magnitude and differ in phase by $\pi/2$. These last equations can be simplified by multiplying the numerator and denominator by the complex conjugate, and using Euler's identity for complex exponentials, resulting in

$$iB_x' = B_z' = \frac{\mu_o B\sigma C}{2} (\frac{1}{k_x^2+\delta^2}) e^{-k_x(h+z)} e^{-i\omega t} [\; (-k_x \sin\delta z - \delta\cos\delta z) 2i\cos\gamma\cos\phi \; + \qquad \textbf{(139)}$$

$$+ \; (-k_x \cos\delta z + \delta\sin\delta z) \frac{2\delta\sin\phi}{k_x} \;] \; \Big|_{D_o}^{D}. \qquad \textbf{(140)}$$

B. CALCULATION OF TURBULENCE INDUCED MAGNETIC FIELD

The integrations for the components of the turbulence induced magnetic field are shown below.

$$B_x' = \frac{\mu_o \sigma B}{4\pi} \int_{x=-\infty}^{x=\infty} \int_{y=-\infty}^{y=\infty} \int_{z=D_o+h}^{z=D+h} \frac{-v_o e^{-i\omega t}}{\sqrt{k_o^2+k_x^2}\sqrt{\omega_o^2+\omega^2}} \frac{e^{ik_x x}}{(x^2+y^2+z^2)^{3/2}}\, dxdydz, \quad \textbf{(141)}$$

$$= \frac{\mu_o \sigma B}{4\pi} \int_{x=-\infty}^{x=\infty} \int_{z=D_o+h}^{z=D+h} \frac{-V_o}{\sqrt{k_o^2+k_x^2}} \int_{y=0}^{y=\infty} \frac{2\, dy}{(x^2+y^2+z^2)^{3/2}}\, dydz, \quad \textbf{(142)}$$

$$= \frac{-2\mu_o \sigma B v_o e^{-i\omega t}}{4\pi\sqrt{k_o^2+k_x^2}\sqrt{\omega_o^2+\omega^2}} \int_{z=D_o+h}^{z=D+h} z \int_{x=-\infty}^{x=\infty} \frac{e^{ik_x x}}{(x+iz)(x-iz)}\, dxdz, \quad \textbf{(143)}$$

$$= \frac{-2\mu_o \sigma B v_o e^{-i\omega t}}{4\pi\sqrt{k_o^2+k_x^2}\sqrt{\omega_o^2+\omega^2}} \int_{x=-\infty}^{x=\infty} \int_{z=D_o+h}^{z=D+h} \frac{z\ e^{-k_x x}}{(x^2+z^2)}\, dxdz. \quad \textbf{(144)}$$

Perform x-integration in upper half of complex plane

$$B_x' = \frac{-2\mu_o \sigma B v_o}{4\pi\sqrt{k_o^2+k_x^2}}\, \pi \int_{z=D_o+h}^{z=D+h} e^{-k_x z}\, dz, \quad \textbf{(145)}$$

$$= \frac{\mu_o \sigma B v_o}{2k_x\sqrt{k_o^2+k_x^2}}\, e^{-k_x h}\, [e^{-k_x D_o} - e^{-k_x D}]. \quad \textbf{(146)}$$

The integration for the y-component is performed in the exact same manner, with x and y interchanged.

The z-component integration is calculated similarly

$$B_z' = \frac{\mu_o \sigma B}{4\pi} \int_{x=-\infty}^{x=\infty} \int_{y=-\infty}^{y=\infty} \int_{z=D_o+h}^{z=D+h} \left[\frac{v_o e^{-i\omega t} x e^{ik_x x}}{\sqrt{\omega_o^2+\omega^2}\sqrt{k_o^2+k_x^2}\,(x^2+y^2+z^2)^{3/2}} + \frac{v_o e^{-i\omega t} y e^{ik_y y}}{\sqrt{\omega_o^2+\omega^2}\sqrt{k_o^2+k_y^2}\,(x^2+y^2+z^2)^{3/2}} \right], \quad \textbf{(147)}$$

$$= \frac{\mu_o \sigma B v_o e^{-i\omega t}}{4\pi\sqrt{\omega_o^2+\omega^2}} \int_{z=D_o+h}^{D+h} [\int_{x=-\infty}^{x=\infty}\int_{y=0}^{y=\infty} \frac{2xe^{ik_x x}dxdydz}{\sqrt{k_o^2+k_x^2}\,(x^2+y^2+z^2)^{3/2}} + \int_{y=-\infty}^{y=\infty}\int_{x=0}^{x=\infty} \frac{2ye^{ik_y y}dxdydz}{\sqrt{k_o^2+k_y^2}\,((x^2+y^2+z^2)^{3/2}}], \quad (148)$$

$$= \frac{2\mu_o \sigma B v_o e^{-i\omega t}}{4\pi\sqrt{\omega_o^2+\omega^2}} \int_{z=D_o+h}^{z=D+h} [\int_{x=-\infty}^{x=\infty} \frac{x\ e^{ik_x x}dxdz}{\sqrt{k_o^2+k_x^2}\,(x^2+z^2)} + \int_{y=-\infty}^{y=\infty} \frac{y\ e^{ik_y y}dydz}{\sqrt{k_o^2+k_y^2}\,(y^2+z^2)}], \quad (149)$$

$$= \frac{2\mu_o \sigma B v_o e^{-i\omega t}}{4\pi\sqrt{\omega_o^2+\omega^2}} \int_{z=D_o+h}^{z=D+h} [\int_{x=-\infty}^{x=\infty} \frac{x\ e^{ik_x x}dxdz}{\sqrt{k_o^2+k_x^2}\,(x+iz)(x-iz)} + \int_{y=-\infty}^{y=\infty} \frac{y\ e^{ik_y y}dydz}{\sqrt{k_o^2+k_y^2}\,(y+iz)(y-iz)}], \quad (150)$$

$$= \frac{2\mu_o \sigma B v_o e^{-i\omega t}}{4\pi\sqrt{\omega_o^2+\omega^2}} \int_{z=D_o+h}^{z=D+h} [\frac{\pi i e^{-k_x z}}{\sqrt{k_o^2+k_x^2}} + \frac{\pi i e^{-k_y z}}{\sqrt{k_o^2+k_y^2}}]\, dz, \quad (151)$$

$$= \frac{\mu_o \sigma B v_o e^{-i\omega t}}{2\sqrt{\omega_o^2+\omega^2}} [\frac{e^{-k_x h}(e^{-k_x D_o} - e^{-k_x D})}{k_x\sqrt{k_o^2+k_x^2}} + \frac{e^{-k_y h}(e^{-k_y D_o} - e^{-k_y D})}{k_y\sqrt{k_o^2+k_y^2}}]. \quad (152)$$

C. INTERNAL WAVE VELOCITY POWER SPECTRAL DENSITY MEASUREMENTS

Data from the Coordinated Eastern Arctic Experiment (CEAREX), March-April 1989.

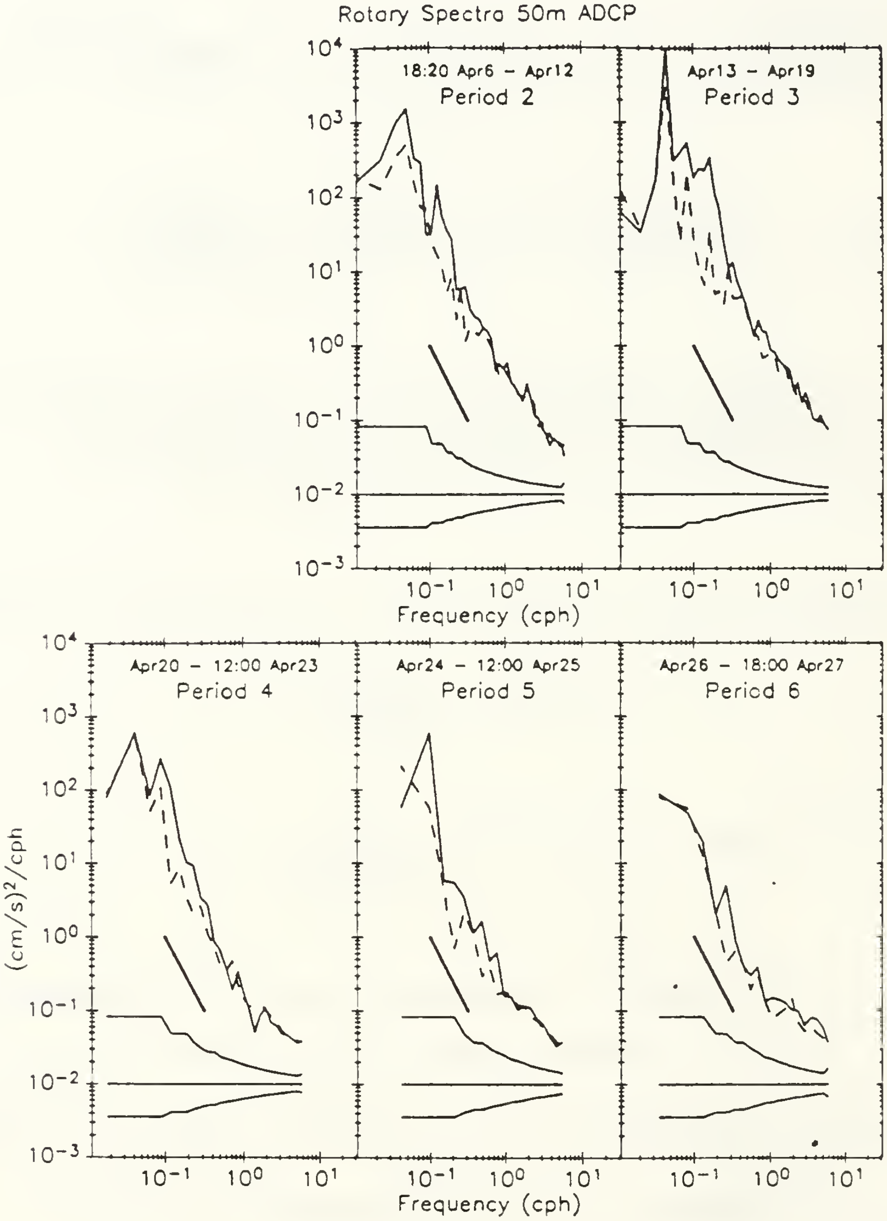

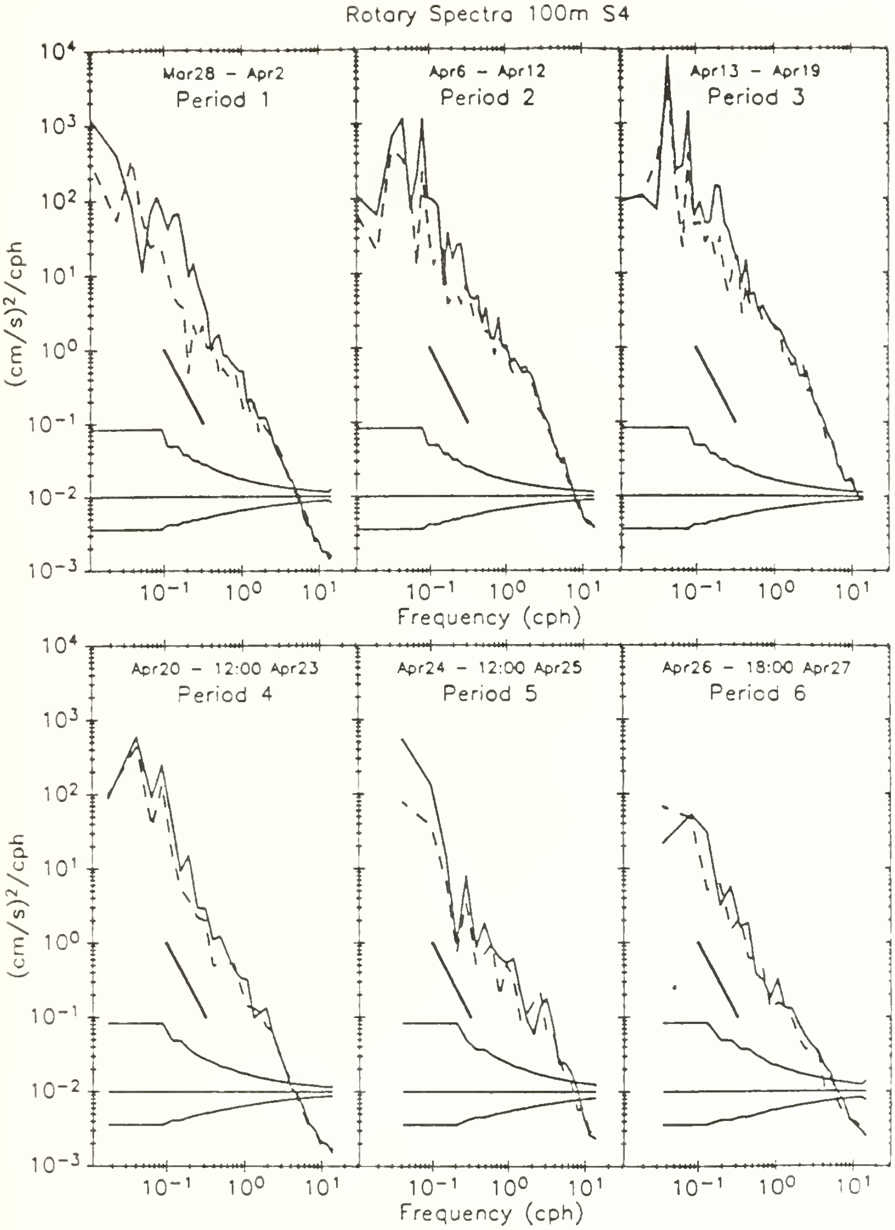
Rotary Spectra 100m S4
Mar28 – Apr2
Period 1
Apr6 – Apr12
Period 2
Apr13 – Apr19
Period 3
Apr20 – 12:00 Apr23
Period 4
Apr24 – 12:00 Apr25
Period 5
Apr26 – 18:00 Apr27
Period 6
(cm/s)^2/cph
10^4
10^3
10^2
10^1
10^0
10^{-1}
10^{-2}
10^{-3}
10^{-1}
10^0
10^1
Frequency (cph)

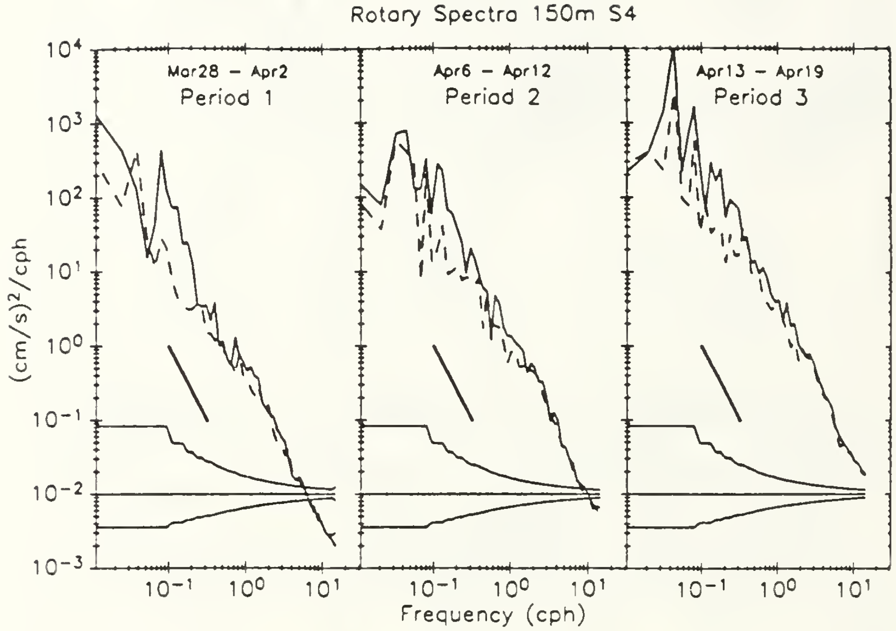
Rotary Spectra 150m S4
Mar28 – Apr2
Period 1
Apr6 – Apr12
Period 2
Apr13 – Apr19
Period 3
(cm/s)^2/cph
10^4
10^3
10^2
10^1
10^0
10^{-1}
10^{-2}
10^{-3}
10^{-1}
10^0
10^1
Frequency (cph)

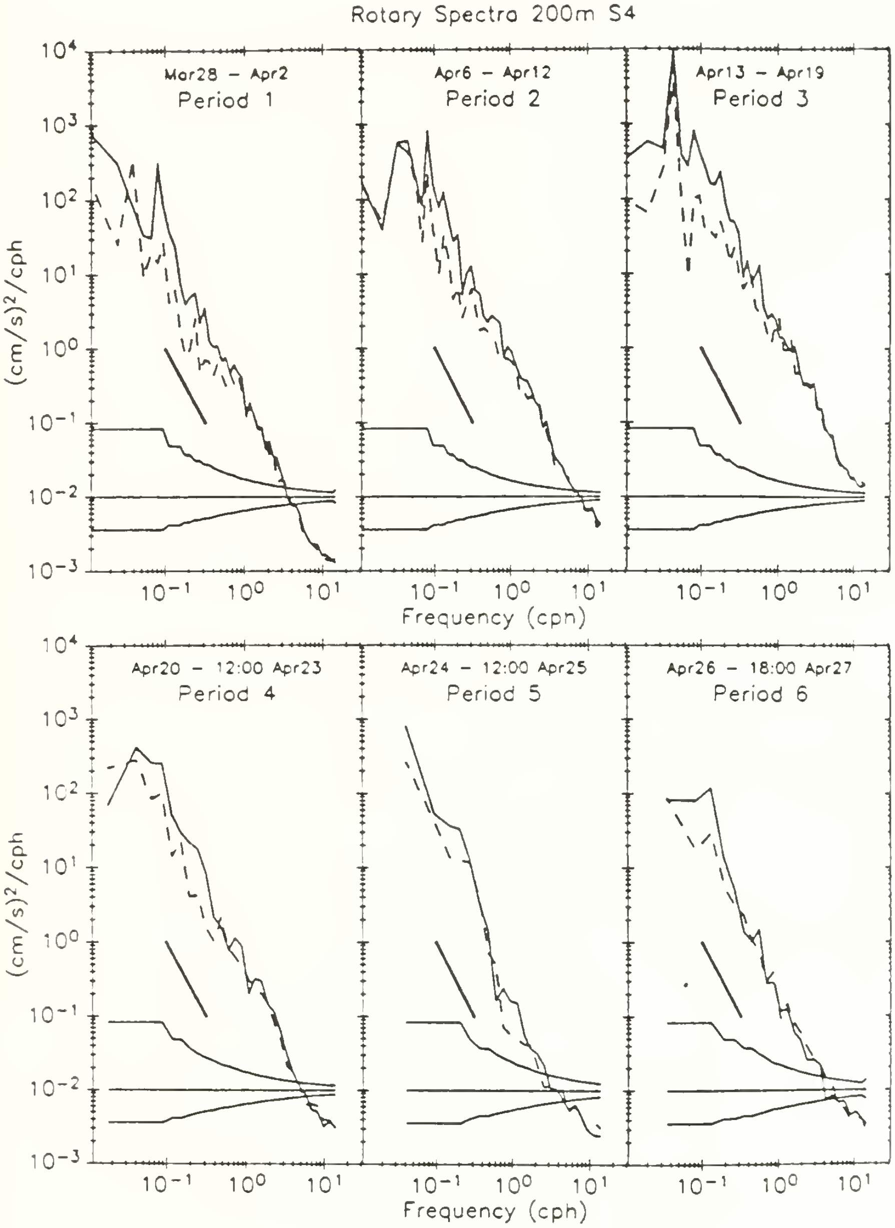
Rotary Spectra 200m S4
Mar28 – Apr2
Period 1
Apr6 – Apr12
Period 2
Apr13 – Apr19
Period 3
Apr20 – 12:00 Apr23
Period 4
Apr24 – 12:00 Apr25
Period 5
Apr26 – 18:00 Apr27
Period 6
10^4
10^3
10^2
10^1
10^0
10^{-1}
10^{-2}
10^{-3}
(cm/s)^2/cph
10^{-1}
10^0
10^1
Frequency (cph)

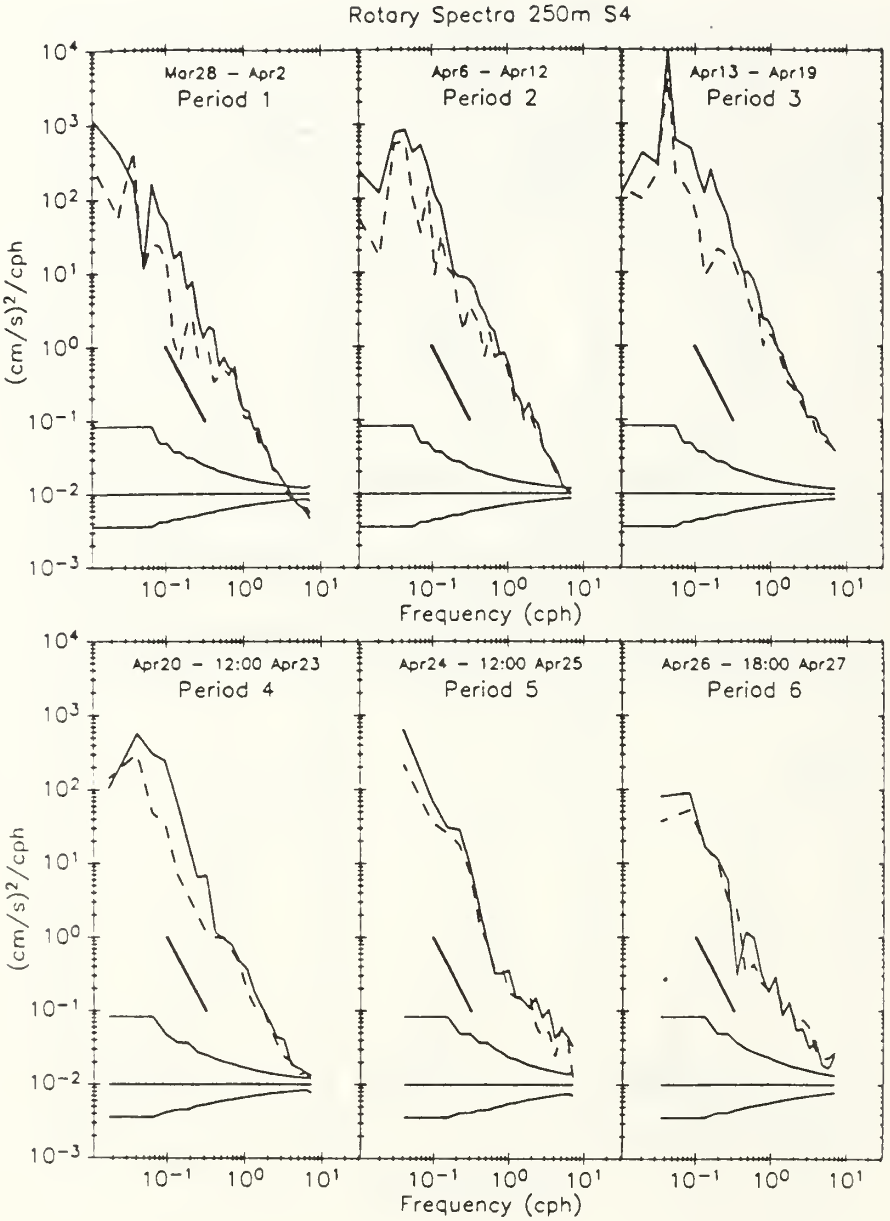
Rotary Spectra 250m S4
Mar28 – Apr2
Period 1
Apr6 – Apr12
Period 2
Apr13 – Apr19
Period 3
Apr20 – 12:00 Apr23
Period 4
Apr24 – 12:00 Apr25
Period 5
Apr26 – 18:00 Apr27
Period 6
(cm/s)²/cph
10⁴
10³
10²
10¹
10⁰
10⁻¹
10⁻²
10⁻³
Frequency (cph)
10⁻¹
10⁰
10¹

D. 1-D TO 2-D POWER SPECTRUM CONVERSION CALCULATION

The one-dimensional power spectrum and its derivative are

$$f_1(k_1) = \frac{1}{k_1^4}, \qquad \frac{d\, f_1(k_1)}{dk_1} = -4\frac{1}{k_1^5}. \tag{153}$$

The two-dimensional power spectrum is given by

$$f_2(k) = -\frac{1}{\pi}\int_k^\infty \frac{d\, f_1(k_1)}{dk_1} \frac{dk_1}{\sqrt{k_1^2 - k^2}}, \tag{154}$$

$$= -\frac{1}{\pi}\int_k^\infty \frac{-4}{k_1^5} \frac{dk_1}{\sqrt{k_1^2 - k^2}}, \tag{155}$$

Make a change of variable

$$m \equiv \frac{k}{k_1}, \qquad k_1 = \frac{k}{m}, \qquad dk_1 = -\frac{k}{m^2}dm, \tag{156}$$

$$f_2(k) = -\frac{4}{\pi}\frac{1}{k^5}\int_0^1 \frac{m^4\,dm}{\sqrt{1-m^2}}. \tag{157}$$

From CRC Standard Math Tables (1987), given a trinomial in m, M = a + bm + cm^2, then

$$\int \frac{m^n}{\sqrt{M}}dm = \frac{1}{nc}m^{n-1}\sqrt{M} - \frac{(2n-1)b}{2nc}\int\frac{m^{n-1}}{\sqrt{M}}dm - \frac{(n-1)a}{nc}\int\frac{m^{n-2}}{\sqrt{M}}dm. \tag{158}$$

Here, a=1, b=0, c=-1. Applying this integral twice yields

$$f_2(k) = -\frac{4}{\pi k^5}\left[-\frac{m^3\sqrt{1-m^2}}{4} - \frac{3m\sqrt{1-m^2}}{8} + \frac{3}{8}\sin^{-1}m \right]_1^0, \tag{159}$$

$$f_2(k) = \frac{3}{4}\frac{1}{k^5}. \tag{160}$$

LIST OF REFERENCES

Beal, H. T. and Weaver, J. T., "Calculations of Magnetic Variations Induced by Internal Ocean Waves," *Journal of Geophysical Research*, v. 75, no. 33, pp. 6486-6852, 20 November 1970.

Berg, P., and McGregor, J., *Elementary Partial differential Equations*, Holden-Day, 1966.

Boas, M. L., *Mathematical Methods in the Physical Sciences*, 2nd ed., John Wiley & Sons, Inc., 1983.

Brigham, E. O., *The Fast Fourier Transform and its Applications*, Prentice-Hall, Inc., 1988.

Chave, A. D., "On the Electromagnetic Fields Induced by Oceanic Internal Waves," *Journal of Geophysical Research*, v. 89, no. C6, pp. 10519-10528, 20 November 1984.

Condon, E., and Odishaw, H., *Handbook of Physics*, McGraw-Hill, 1967.

CRC Handbook of Chemistry and Physics, 62nd ed., pp. F-3,F-166, CRC Press, Inc., 1981.

CRC Standard Mathematical Tables, 28th ed., CRC Press, Inc., 1987.

Crews, A. and Futterman, J., "Geomagnetic Micropulsations Due to the Motion of Ocean Waves," *Journal of Geophysical Research*, v. 67, no. 1, pp. 299-306, January, 1962.

Czipott, P. V. and Podney, W. N., "Measurement of magnetic Fluctuations above the Arctic Ocean during Project AIWEX: Experiment Description and Data Overview," technical report for Physical Dynamics, Inc., 1985.

D'Asaro, E., and Morehead, M., "*Internal Waves and Velocity Fine Structure in the Arctic Ocean*", Journal of Geophysical Research, v. 96, no. C7, pp. 12,725-12,738, July 15, 1991.

Dietrich, Kalle, Krauss, and Siedler, *General Oceanography*, 2nd ed., p. 62, plates 3-5, John Wiley & Sons, Inc., 1980.

Garrett, C. and Munk, W., "Space-Time Scales of Internal Waves," *Geophysical Fluid Dynamics*, v. 2, pp. 225-264, 1972.

Gill, A. E., *Atmosphere-Ocean Dynamics,* Academic Press, Inc.,1982.

Gradshteyn, I. S. and Ryzhik, I. M., *Table of Integrals, Series, and Products*, Academic Press, Inc., 1965.

Gray, D. E., *American Institute of Physics Handbook*, McGraw-Hill, 1972.

Gross, M. C., Oceanography, A View of the Earth, pp. 156-160, Prentice-Hall, Inc., 1972.

Kraichman, M. B., *Handbook of Electromagnetic Propagation in Conducting Media*, U.S. Government Printing Office, Washington, DC, 1976.

Levine, M., Paulson, C., and Morison, J., "*Observations of Internal Gravity Waves Under the Arctic Pack Ice*", Journal of Geophysical Research, v. 92, no. C1, pp. 779-782, January 15, 1987.

McPhee M., "*A Rigid, Cable-Lowered Instrument Frame for Measuring Turbulence and Internal Waves in the Arctic*", IEEE Journal of Oceanic Engineering, v. 14, no. 2, pp. 203-207, April 1989.

Office of Naval Research, Data Report 152, *Observations from CEAREX "O" Camp, Arctic Ocean, March-April 1989*, by Levine, M., Paulson, C., Simpkins, J., and Gard, S., Reference 91-1, April 1991.

Parkinson, *Introduction to Geomagnetism*, pp. 72-76, University Press, 1983.

Peerless, S. J., *Basic Fluid Mechanics*, Pergamon Press, 1967.

Petersen, R. A. and Poehls, K. A., "Model Spectrum of magnetic Induction Caused by Ambient Internal Waves," *Journal of Geophysical Research*, v. 87, no. C1, pp. 433-440, 20 January 1982.

Phillips, O. M., *The Dynamics of the Upper Ocean*, Cambridge University Press, 1969.

Podney, W., "Electromagnetic Fields Generated by Ocean Waves," *Journal of Geophysical Research*, v. 80, no. 21, pp. 2977-2990, 20 July 1975.

Podney, W. and Sager, R., "Measurement of fluctuating magnetic gradients Originating from Oceanic Internal Waves," *Science*, v. 205, pp. 1381-1382, 28 September 1979.

Sommerfeld, A. W., *Electrodynamics, Lectures on Theoretical Physics,* v. 2, pp. 280-283, Academic Press, Inc., 1952.

Stanton, T., Adjunct Resident Professor, Oceanography, Naval Postgraduate School; conversation with, 11 December 1991.

Tatarski, V. I., *Wave Propagation in a Turbulent Medium*, McGraw-Hill Book Company, Inc., 1961.

Warburton, F. and Caminiti, R., "The Induced Magnetic field of Sea Waves," *Journal of Geophysical Research*, v. 69, no. 20, pp. 4311-4318, 15 October 1964.

Weaver, J. T., "Magnetic Variations Associated with Ocean Waves and Swell," *Journal of Geophysical Research*, v. 70, pp. 1921-1929, 1965.

Yaglom, A. M., *Correlation Theory of Stationary and Related Random Functions, Vol. I: Basic Results*, Springer-Verlag, 1987.

INITIAL DISTRIBUTION LIST

1.	Library, Code 52 Naval Postgraduate School Monterey, CA 93943-5002	2
2.	Prof. Donald L. Walters Department of Physics (Code PH/We) Naval Postgraduate School Monterey, CA 93943-5004	5
3.	Prof. Xavier K. Maruyama Department of Physics (Code PH/Mx) Naval Postgraduate School Monterey, CA 93943-5004	1
4.	Prof. Karlheinz E. Woehler Department of Physics (Code PH/Wh) Naval Postgraduate School Monterey, CA 93943-5004	1
5.	Prof. Timothy P. Stanton Department of Oceanography (Code OC/St) Naval Postgraduate School Monterey, CA 93943-5004	1
6.	Dr. Harvey W. Ko The Johns Hopkins University Applied Physics Laboratory Johns Hopkins Road Laurel, Md 20723-6099	1

846-217

Thesis
D169523 Davis
c.1 Magnetic fields generated by internal ocean seawater motion.

AMERICAN BINDERY
2
9-93

DUDLEY KNOX LIBRARY
3 2768 00034214 1